

MODELING THE FLOW OF A LIQUID DROPLET DIFFUSING INTO VARIOUS  
POROUS MEDIA FOR INKJET PRINTING APPLICATIONS

By

SARAH ROSE SUFFIELD

A thesis submitted in partial fulfillment of  
the requirements for the degree of

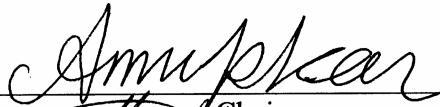


MASTER OF SCIENCE IN MECHANICAL ENGINEERING

WASHINGTON STATE UNIVERSITY VANCOUVER  
School of Engineering and Computer Science

MAY 2008

To the Faculty of Washington State University:

The members of the Committee appointed to examine the dissertation/thesis of SARAH ROSE SUFFIELD find it satisfactory and recommend that it be accepted.

  
Chair  
  


## ACKNOWLEDGMENT

I would like to acknowledge and thank my advisor, Dr. Amir Jokar. I am very grateful for the time he took to help me with this project. Without his guidance and knowledge the completion of this thesis would not have been possible.

I would also like to thank my employer, HP, who provided financial support for my graduate education. HP also provided me with the equipment resources required for this project. I am also extremely appreciative of all the support I received from my managers and coworkers. Without their understanding around my flexible work schedule, completion of my masters degree would not have been possible.

# MODELING THE FLOW OF A LIQUID DROPLET IMPACTING WITH VARIOUS POROUS MEDIA FOR INKJET PRINTING APPLICATIONS

Abstract

by Sarah Rose Suffield  
Washington State University  
May 2008

Chair: Amir Jokar

Inkjet technology currently relies heavily upon the absorption of ink into porous media. Characterizing the absorption capacity of media as well as the absorption rate can be critical in understanding the entire drying process. Evaluating the absorption performance of a coated medium can particularly be important since the coating may be either semi-absorptive, or in some cases non-absorptive. The absorption performance can also vary among uncoated media. In order to better understand the absorption mechanism, the fluid flow of a liquid droplet impacting with several porous papers, each with a unique permeability was analyzed numerically and experimentally in this study. The droplet impact was simulated by the computational fluid dynamics (CFD) technique for a variety of conditions. The transient CFD modeling predicted the shape of the droplet at different time intervals before and after the impact. It also predicted the volume of liquid that had diffused into the porous substrate over time. The results predicted by the CFD model were then compared to experimental data, which was collected for a real system with the same configuration as in the CFD modeling, using a high speed digital video camera. The camera captured images of a droplet as it impacted with various coated and uncoated papers. Results showed a relatively good agreement between the computational modeling and experimentation at drop times greater than 0.1 seconds after the impact. A dimensional analysis was also performed on the most effective parameters of the flow process, and an imperial correlation was developed to predict the aspect ratio of the droplet after the impact as a function of the other dimensionless parameters, such as Reynolds and Weber numbers. The results of this

study can be useful for drying applications, such as inkjet printing, where absorption of a liquid into a porous medium is critical for the drying process.

## TABLE OF CONTENTS

	Page
ACKNOWLEDGEMENTS .....	iii
ABSTRACT .....	iv
LIST OF TABLES .....	ix
LIST OF FIGURES .....	x
NOMENCLATURE .....	xii
CHAPTER	
1. INTRODUCTION .....	1
2. LITERARY REVIEW .....	4
Porosity and Permeability .....	4
Surface Tension .....	7
System Modeling .....	7
3. CFD SIMULATION .....	11
System Introduction .....	11
System Geometry .....	12
Mesh .....	12
Boundary Conditions .....	14
Fluent Models .....	15
Fluent Solver .....	17
Input Data .....	18
Property Calculations .....	19
Porosity and Permeability .....	19
Anisotropic Permeability .....	23
Surface Tension .....	24
Droplet Velocity .....	25

Media .....	26
CFD Results .....	27
Volume of Water within Media .....	27
Aspect Ratio .....	29
4. EXPERIMENTAL TEST FACILITY .....	31
Experimental Schematic .....	31
Syringe .....	33
Fixture .....	33
Camera and Lens .....	33
Other Equipment .....	33
Test Procedure .....	36
5. EXPERIMENTAL RESULTS AND COMPARISONS .....	37
Calculated Properties .....	37
Contact Angle .....	37
Average and Impact Velocity .....	38
Aspect Ratio .....	39
Data Comparisons .....	39
6. DIMENSIONAL AND UNCERTAINTY ANALYSIS .....	45
Dimensional Analysis .....	45
Derive Pi Terms .....	46
Aspect Ratio Correlation .....	46
Uncertainty Analysis .....	49
Uncertainty Results .....	50
7. SUMMARY AND CONCLUSIONS .....	52
BIBLIOGRAPHY .....	54
APPENDIX	
A. INERTIAL RESISTANCE FOR UNCOATED MEDIA .....	56

B. SURFACE TENSION AT SUBSTRATE/AIR INTERFACE .....	57
C. DIMENSIONAL ANALYSIS .....	59
D. ASPECT RATIO CORRELATION .....	63
E. VISUAL BASIC CODE FOR UNCERTAINTY.....	65



## LIST OF TABLES

1. Tabulated Permeability Data for Cellulose Fibers .....	19
2. Media Set .....	27
3. Average Contact Angle .....	38
4. Estimated Uncertainty of Parameters .....	51

## LIST OF FIGURES

1. Major Paper Directions .....	6
2. Flow Diagram of a Droplet Impacting with a Porous Medium .....	12
3. Model Geometry .....	13
4. Typical Mesh Plot .....	14
5. Plot of Tabulated Cellulose Permeability Data .....	20
6. Permeability Direction Vectors in Fluent Model .....	24
7. Volume of Water Absorbed from the CFD Model for Uncoated Media ....	28
8. Volume of Water Absorbed from the CFD Model for Coated Media .....	29
9. CFD Aspect Ratio for Uncoated Media .....	30
10. CFD Aspect Ratio for Coated Media .....	30
11. Experimental Schematic .....	32
12. Close Up View of Syringe/Lens Setup .....	32
13. Media Thickness Image of M2 .....	34
14. Coating Thickness Image of M1 .....	35
15. Fiber Diameter Image for M2 .....	36
16. Contact Angle Image for M2 .....	37
17. Aspect Ratio Comparison of M1 .....	39
18. Aspect Ratio Comparison of M2 .....	40
19. Aspect Ratio Comparison of M3 .....	40
20. Aspect Ratio Comparison of M4 .....	41
21. CFD Model Aspect Ratio Deviation $< 0.1$ Seconds after Impact .....	42
22. CFD Model Aspect Ratio Deviation $\geq 0.1$ Seconds after Impact .....	42
23. CFD at 0.005 seconds .....	43
24. Experiment at 0.005 seconds .....	43
25. CFD at 0.01 seconds .....	43

26. Experiment at 0.01 seconds .....	43
27. CFD at 0.02 seconds .....	44
28. Experiment at 0.02 seconds .....	44
29. CFD at 0.1 seconds .....	44
30. Experiment at 0.1 seconds .....	44
31. $\pi_2$ versus $\pi_7$ for various Weber numbers and porosities .....	47
32. $\pi_2$ versus $\pi_7$ for various Reynolds numbers .....	47
33. Percent Deviation of Aspect Ratio Correlation .....	49

## NOMENCLATURE:

$a$  : fiber diameter (m)

$a_g$  : acceleration due to gravity ( $\text{m/s}^2$ )

$a_L$  : electric polarisability of liquid

$a_S$  : electric polarisability of substrate

$A_S$  : surface area of medium sample ( $\text{m}^2$ )

$C$  : constant

$C_2$  : inertial resistance coefficient (1/m)

$d$  : drop diameter after impact (m)

$D$  : drop diameter before impact (m)

$D_{pipe}$  : nozzle diameter (m)

$D_x$  : fiber or particle diameter (m)

$f_i$  : system equation

$\overline{f}$  : mean value for system equation

$F_a$  : fiber aspect ratio

$G$  : basis weight of the medium ( $\text{g/m}^2$ )

$H$  : total drop distance between droplet and medium (m)

$H'$  : drop height as it approaches the medium (m)

$h$  : drop height after impact (m)

$I$  : turbulence intensity

$k$  : constant

$K_L'$  : adjusted loss factor

$K_L$  : loss factor

$\ell$  : turbulence length scale (m)

$L_B$  : base layer thickness of the medium (m)

$L_C$  : coated thickness of the medium (m)

$L_m$  : total thickness of the medium (m)

$m$  : number of experimental runs  
 $M1$  : medium one (coated)  
 $M2$  : medium two (uncoated)  
 $M3$  : medium three (uncoated)  
 $M4$  : medium four (uncoated)  
 $n$  : number of coating layers  
 $P$  : dimensionless permeability number  
 $r$  : aspect ratio  
 $r_{CFD}$  : aspect ratio from the CFD model  
 $r_{EXP}$  : aspect ratio from the experimental data  
 $Re$  : Reynolds number  
 $S$  : spreading parameter  
 $Si$  : source term ( $N/ m^3$ )  
 $t$  : time after impact (s)  
 $t_d$  : droplet fall time (s)  
 $U_D$  : uncertainty of droplet diameter before impact (%)  
 $U_H$  : uncertainty of distance between droplet and medium (%)  
 $U_h$  : uncertainty of droplet height after impact (%)  
 $U_t$  : uncertainty of time after impact (%)  
 $U_v$  : uncertainty of droplet velocity (%)  
 $U_\varepsilon$  : uncertainty of porosity (%)  
 $U_\rho$  : uncertainty of density (%)  
 $U_\sigma$  : uncertainty of surface tension between medium and fluid (%)  
 $U_\mu$  : uncertainty of viscosity (%)  
 $U_{\pi_2}$  : uncertainty of aspect ratio (%)  
 $v_i$  : fluid velocity in the  $i^{th}$  direction (m/s)  
 $v_{imp}$  : fluid velocity at impact with the medium (m/s)

$v_m$  : magnitude of fluid velocity (m/s)  
 $v_o$  : initial droplet velocity at the nozzle (m/s)  
 $v_{open}$  : velocity for 100% open area flow (m/s)  
 $v_{pb}$  : velocity for partially blocked flow in the porous region (m/s)  
 $V$  : average drop velocity (m/s)  
 $V_{LL}$  : van der Waal energy between two like liquids (dynes/cm)  
 $V_{SL}$  : van der Waal energy between the substrate and liquid (dynes/cm)  
 $V_{SS}$  : van der Waal energy between two like substrates (dynes/cm)  
 $VR$  : viscous resistance coefficient (1/m<sup>2</sup>)  
 $W_{dry}$  : dry weight of the medium sample (kg)  
 $We$  : Weber number

#### **GREEK SYMBOLS:**

$\alpha$ : permeability of the medium (m<sup>2</sup>)  
 $\epsilon$ : porosity, or void fraction  
 $\theta$ : contact angle (degrees)  
 $\kappa$ : turbulent kinetic energy (m<sup>2</sup>/s<sup>2</sup>)  
 $\mu$ : viscosity (kg/m-s)  
 $\rho$ : density (kg/m<sup>3</sup>)  
 $\rho_s$  : density of solid medium material (kg/m<sup>3</sup>)  
 $\sigma_{LA}$  : surface tension coefficient between liquid and air (dynes/cm)  
 $\sigma_{SA}$  : surface tension coefficient between substrate and air (dynes/cm)  
 $\sigma_{SL}$  : surface tension coefficient between substrate and liquid (dynes/cm)  
 $\Phi$ : solid volume fraction  
 $\omega$ : specific momentum dissipation rate (m/s)

## **Dedication**

This thesis is dedicated to my mother and father who have  
always supported my educational pursuits.

## **CHAPTER ONE**

### **INTRODUCTION**

There are two main mechanisms that can be used in inkjet printing: 1) diffusing ink into the porous medium, and 2) drying ink on the porous medium through an evaporation process. Inkjet technology currently relies heavily upon the first mechanism, i.e., absorption of ink by a porous substrate. Characterizing the capacity of a medium in absorbing ink as well as the absorption rate can be important to understand if any additional drying is required. Evaluating the absorption performance can particularly be important for coated media, which may be either semi-absorptive or in some cases non-absorptive. The absorption performance can also vary among uncoated media. Additionally, convective drying can happen in inkjet printing that drives water from the medium through an evaporation process. Varying the amount of time a medium is exposed to the dryer subsystem allows media with greater drying requirements to dwell longer within the heater subsystem in order to increase the drying rate. It is essential to characterize the absorption performance of a medium first to better understand the overall drying requirements for that medium.

The fluid flow of a liquid droplet impacting papers with different porosities was simulated using computational fluid dynamics (CFD) techniques. The method was accomplished using the software package Fluent. Using the volume of fluid (VOF) and porous medium models within Fluent, a transient CFD model was created. The model predicted the shape of the droplet at different time intervals before and after the impact with the porous medium. The CFD model also predicted the volume of liquid that had diffused into the medium over time.

An experiment was then set up to capture images of a water droplet impacting with various porous papers. The droplet was ejected from a syringe, and a high speed camera recorded images of the droplet colliding with the medium. Four different porous



media were tested. Three of the media tested were various versions of uncoated plain paper. The remaining medium was a porous coated medium. The coated medium was designed to work with an inkjet paper and thus had a highly porous coating layer.

A dimensional analysis was also performed on the droplet/medium interactions. Using the Buckingham Pi theorem, seven non-dimensional terms were defined. The non-dimensional terms, along with the experimental data that had been collected, were used to develop an equation to predict the aspect ratio of the droplet. The results predicted by both the dimensional analysis and CFD model for the droplet aspect ratio were compared to experimental data. The results of the computational modeling and dimensional analysis could be useful to drying applications, such as inkjet printing, where absorption of a liquid into a porous substrate is critical for drying.

An extensive literary review was conducted and is presented in chapter two of this thesis. Previous papers looking at how to determine the porosity and permeability of a medium were studied. Surface tension was also expected to be an important parameter involved in the droplet/medium interaction. Thus prior work looking at the surface tension between a liquid and porous substrate was examined, along with previous system modeling.

After presenting the previous work that was examined, an introduction to the droplet system under study is presented in chapter three along with a detailed description of the system geometry. Chapter three also introduces the CFD modeling that was conducted over the course of the project. The commercial software package, Fluent, was used to model the system, and thus background information on the models used within Fluent is given, along with information about the mesh and boundary conditions used. The approaches used to calculate the required input parameters to the Fluent model are also given in chapter three. Results from the CFD model are presented. The results included characterizing the droplet's geometry after impact, and the volume of water that has been absorbed by the medium.

In addition to the modeling, an experiment was set up to capture images of a droplet impacting with various media. Chapter four introduces the equipment and procedure used in the experiment. The various media used in the experiment is also detailed in chapter six.

The results of the experiment are then presented in chapter five. Details regarding the procedures used to determine the droplet velocity and contact angle using the camera images are also presented. Chapter five also compares the experiment results with the CFD results.

A dimensional analysis of the droplet system was conducted and is presented in chapter six. Using experimental data and the pi terms calculated from the dimensional analysis, a correlation to predict the aspect ratio of the droplet after impact was derived. The uncertainty associated with the aspect ratio correlation is also presented in chapter six. Details of the procedure used to calculate the uncertainty are presented. The uncertainties associated with other important parameters are also given in chapter six.

An overall summary of the research project is presented in chapter seven. The summary highlights the main results of the project. In addition to the summary, a look at the potential industrial applications of the results is also given, along with a few future recommendations.

## **CHAPTER TWO**

### **LITERATURE REVIEW**

This chapter provides a detailed literary review of technical papers that were examined over the course of this research project. Papers pertaining to the porosity and permeability of a medium are presented first, followed by papers on the surface tension between a fluid and porous medium, and finally literature on previous system modeling.

#### **2.1 Porosity and Permeability**

The porosity, also known as the void fraction, is defined as the ratio of open spaces (pores) to the total volume that makes up the medium. The porosity is related to the permeability, which is the medium's ability to transmit fluid through its pores. There are various forms of porous media; one such form is a fibrous mat.

There has been a significant amount of experimentation and research on laminar flow through a fibrous porous medium. Fibrous media are made up of elongated solid particles. The fiber particles do not necessarily need to be straight and could be randomly oriented. Plain, uncoated paper could be considered a fibrous medium. It is usually composed of small cellulose fibers. During the paper making process the fibers become interlaced, forming a mat of paper.

Jackson and James [1986] gathered and examined significant data related to low Reynolds number flow through fibrous media. They were able to characterize and compare the range of experimental data in terms of a dimensionless permeability number ( $P$ ), and the solid volume fraction ( $\phi$ ). It was assumed that all fibers were circular and therefore could be characterized by a single uniform diameter. The data tabulated covers many types of fiber materials; cellulose was not one of the materials, though.

Nilsson and Stenstorm [1997] looked at the permeability of pulp and paper. They used the CFD program FICAP to create a model that predicts the permeability of

cellulose fiber structures, like those found in paper. The permeability values predicted by the FICAP model were compared with experimental data. They looked at both structured and randomly oriented fiber arrangements. Depending on the fiber aspect ratio ( $F_a$ ), the calculated permeability values corresponded very well with the experimental data.

Rioux [2003] determined the permeability of various media using experimental data from a Bristow Absorption Tester. The Bristow tester measured the absorption of a medium by looking at the amount of liquid volume that is transferred from the tester to the medium. He was able to calculate the permeability of an uncoated medium using Darcy's Law to determine a relationship for permeability based on the measured penetration depth from the Bristow tester, along with velocity and pressure difference measurements from a Sheffield-type porosimeter.

Rioux was also able to determine the permeability of a coated medium. A coated medium's permeability was calculated based on a relationship using the total liquid volume (TLV) measured from the Bristow tester along with other important medium parameters such as porosity, pore radius, and contact angle between the medium and fluid. The porosity and pore radius of the coating layer was measured using a mercury porosimeter. A camera was used to capture images of a drop settling on the coated surface. These images were analyzed to determine the contact angle between the medium and fluid.

Ergun [1952] studied the flow of a fluid through a packed bed of granular solids. A packed bed is composed of tiny circular solid particles that are packed tightly together to form a porous medium. The coating layer of a porous medium could be considered a packed bed. He determined that the total energy loss, which results in a pressure drop in the packed bed, can be treated as the sum of viscous and kinetic energy losses. For laminar flow, the kinetic energy loss terms goes to zero.

Lindsay [1990] studied the anisotropic behavior of paper. Three mutually-perpendicular directions were typically used to describe paper: the machine direction, the

cross-web direction, and the transverse direction. During the paper production process, the paper is moved through roller presses, and the direction parallel to the flow of material out of the press is considered the machine direction. The transverse direction was normal to the sheet/paper, while the machine direction and cross-web direction were parallel to the sheet, as presented in Figure 1. The machine and cross-web directions are often referred to as “in-plane” permeability. It is assumed that any differences between the machine and cross-web direction are very small and can be neglected. Thus the in-plane permeability is assumed to be isotropic. This should be a valid assumption since droplets typically spread in a circular fashion when interacting with paper. Any major differences within the in-plane permeabilities would result in non-circular, or anisotropic, droplet spreading.

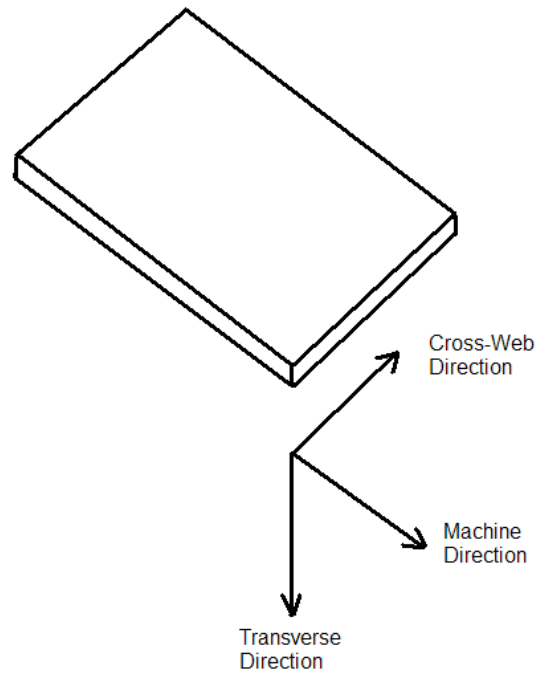


Figure 1: Major Paper Directions

Even though paper is recognized as an anisotropic medium, most permeability measurements have been focused on the transverse direction. Some previous work has

been done though to characterize the differences in permeability between the in-plane and transverse paper directions. Lindsay [1990] used a hydraulic press to measure the lateral and transverse permeabilities under uniform loads. He found the anisotropy ratio of in-plane to transverse permeability to be generally greater than one. Hamlen and Scriven [1991] found that for an uncompressed sheet, the anisotropy ratio is around 5.5.

## **2.2 Surface Tension**

Surface tension is an important physical parameter for the droplet/porous medium interaction. After the initial impact the droplet will wick into the capillary spaces and spread out on the porous medium. De Gennes et al. [2004] determined that the spreading of the droplet can be characterized by the spreading parameter,  $S$ , which is a comparison between the wet and dry surface energy of the substrate. For a droplet on a substrate there are three surface tension coefficients involved: the surface tension at the substrate/air, substrate/liquid, and liquid/air interfaces. The spreading parameter is a function of all three surface tension coefficients. De Gennes et al. [2004] also showed that the surface tension can be related to the van der Waals energy. The van der Waals energies are the result of dispersion forces between molecules. They are the weakest of the intermolecular forces, but they play an important role in surface interactions.

Rioux [2003] also determined contact angle, and thus surface tension, has a significant impact of the physical properties of the water droplet as it impacts and diffuses with the medium. As stated previously, he determined the contact angle through camera images.

## **2.3 System Modeling**

A significant amount of previous research and modeling has been done on droplets impacting with a solid surface. Impact with a porous surface is a more

complicated phenomenon. It involves not only spreading of the droplet along the surface, but also absorption into the permeable surface.

There have been considerable studies' looking at the absorption of a liquid into a porous medium using the Lucas-Washburn equation, which describes the penetration of a liquid into a cylindrical capillary. One such study was done by Mamur and Cohen [1997]. They used the Lucas-Washburn equation to characterize the liquid penetration of porous media. Another study by Hamraoui and Nylander [2002] used an analytical approach to model the diffusion of liquid into a porous structure. The model was based on the Lucas-Washburn equation. These studies neglected inertial effects due to impact forces though.

Numerical models have been developed to simulate flow of a liquid droplet as it impacts with a porous medium. One such model was developed by Hsu and Ashgriz [2004]. Their numerical model simulated a droplet impacting with two parallel plates separated by a specified distance. This specified gap created a radial capillary that drew the droplet towards the cap due to a pressure difference between the internal droplet pressure and the pressure within the gap. The model assumed a free surface condition. A free surface condition occurs when a fluid boundary interfaces with another fluid. The effect of the external fluid upon the motion of the internal fluid is considered negligible. This assumption is valid when the internal fluid has a much larger viscosity and density in comparison with the external fluid. The model also assumed 2-dimensional, incompressible, and transient flow. It also took into account the surface tension at the interface between the liquid and porous substrate. The surface tension was modeled using the continuum surface force (CSF) model.

The Hsu-Ashgriz model used the hydrodynamics code RIPPLE to solve the incompressible Navier-Stokes equations for a rectilinear mesh geometry using a finite difference method. The model used the volume of fluid (VOF) technique to track the position and shape of the droplet. Results of the model showed that the droplet

properties, velocity, contact angle with the substrate, and capillary geometry were important properties related to droplet spreading and absorption.

Reis et al. [2004] also created a numerical model to simulate a liquid droplet impacting with a porous medium. This model also assumed free surface flow for the permeable surface. It took into account inertial effects, surface tension inside and outside the porous medium, pressure at impact, and capillary effects. The model assumed the fluid flow is governed by the continuity of mass and momentum conservation equations. These equations were discretized using the finite volume method. This was done using the SIMPLEC algorithm. Position and geometry of the droplet was tracked using the marker-particle method.

A numerical model was also created by Alam et al. [2007]. Their model and research was mainly focused on how an irregular surface affects the spreading and absorption of an impacting droplet. They did also look at impact with a flat porous surface though. The CFD software FLOW3D was used to create the model, which used the VOF method. The geometry was discretized with a rectilinear mesh and used the finite difference method to solve the Navier-Stokes equations. Values for fluid viscosity, surface tension, capillary pressure, and medium porosity were all input into the model. FLOW3D was able to calculate the contact angle between the fluid and porous medium. Results showed the droplet viscosity, velocity, and pressure outside of the medium to be important parameters. An irregular porous surface resulted in asymmetrical spreading and absorption of the liquid, but a flat profile for the surface resulted in an approximately circular perimeter.

Kannangara et al. [2006] looked at the interactions between a paper surface and a liquid droplet. They used a high-speed CCD camera study the physics of a drop as it impacts with sized paper. The sized papers had different levels of solvent content that made up the cellulose film of the particular paper. Experimental results were compared with the predicted results based on a model developed by Park et al. [2003]. The model



predicted the maximum drop spreading ratio,  $D_m$ , which is the ratio of the maximum drop diameter after impact and the spherical diameter of the drop before impact. The Park et al. model assumes a solid smooth hydrophobic or hydrophilic surface instead of a porous interface. Thus, diffusion into the paper does not appear to be accounted for in this model.

## **CHAPTER THREE**

### **CFD SIMULATION**

CFD modeling was used as a simulation tool to predict the absorption performance of a medium using the Fluent commercial software. The model predicts the shape and velocity of the droplet at different time intervals. It also predicts the time and amount of fluid from the droplet that has diffused into the porous substrate. This chapter describes the CFD model in detail. A detailed description of the system analyzed in this study is also given.

#### **3.1 System Introduction**

In order to better understand the absorption mechanism, a system involving a droplet coming into contact with a porous medium was analyzed. Traditionally ink has a high percentage of water content. Thus for the purposes of this project, the droplet was assumed to be composed of water. The droplet was assumed to be ejected from a nozzle, for this project a syringe nozzle was used.

Various papers intended for use with an inkjet printer were used as the porous substrate with which the droplet collides. All of the media were classified as porous, including the coated medium that was considered. The coated medium was composed of a base layer, which was made up of many cellulose fibers all packed together. Surrounding the base layer was a coating layer on each side. The coating layer was composed of tiny silica particles packed tightly together.

In addition to the coated medium, various uncoated media were also considered. The uncoated, or plain papers, were composed of cellulose fibers matted together, similar to the base layer of the coated medium. Various uncoated papers were tested, with each

one having a unique porosity and permeability value. The permeability is defined as a substrates ability to convey fluid through its pores.

### 3.1.1 System Geometry

The schematic of the system analyzed is shown in Figure 2. A droplet is ejected from a nozzle, with a diameter of  $D_{\text{pipe}}$ . The droplet is ejected with an average velocity  $V$ , a diameter  $D$ , and drops a distance  $H$  before impacting the medium. After impact the height  $h$  and diameter  $d$  are used to characterize the drop geometry after impact.

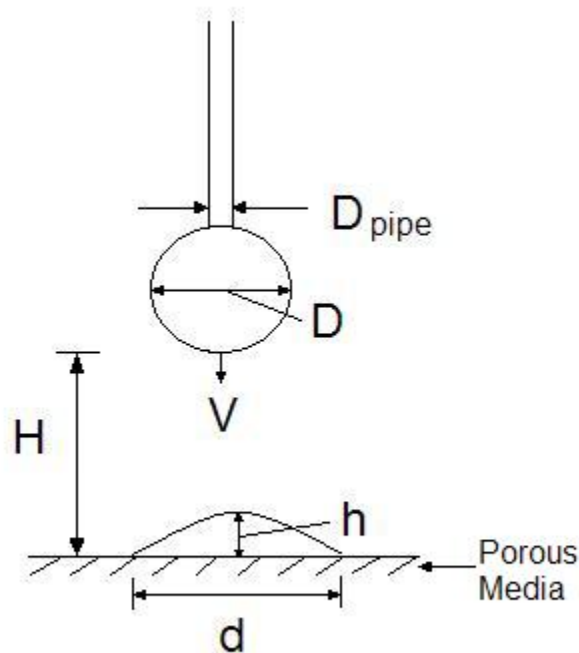


Figure 2: Flow Diagram of a Droplet Impacting with a Porous Medium

### 3.2 Mesh Generation

The geometry of the model is shown in Figure 3. The syringe nozzle has a diameter of 0.5 mm. After being ejected from the nozzle the droplet free falls in the atmosphere until it contacts with the porous medium. The atmospheric interaction is

represented by an air chamber in the model. The porous medium was assumed to have a flat uniform surface.

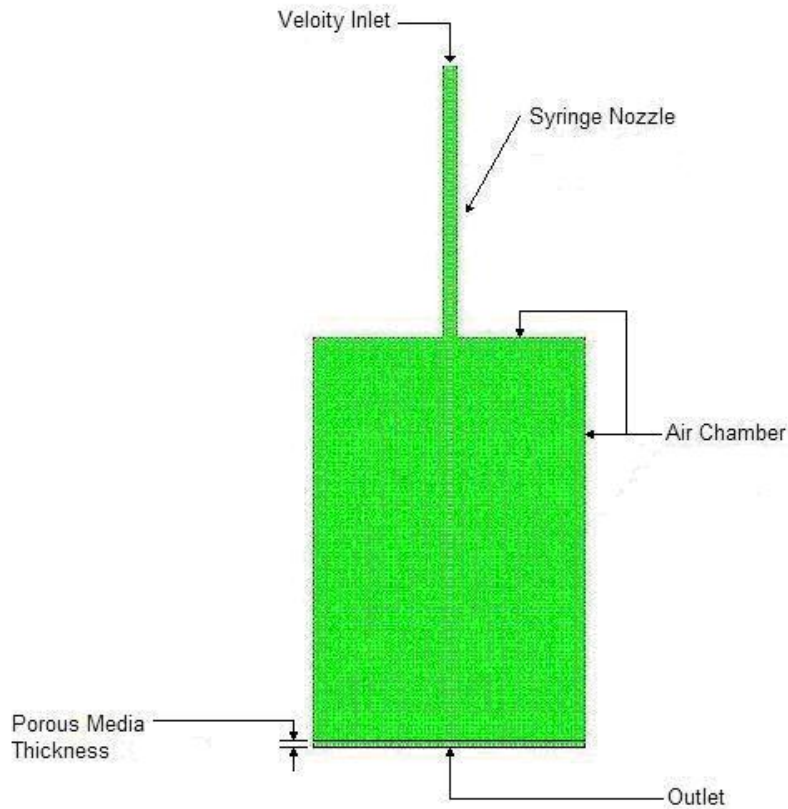


Figure 3: Model Geometry

A symmetrical condition was assumed for the nozzle, air chamber, and porous medium. This reduced the mesh size and computation time. It was also assumed that after impact the droplet spread along the porous surface in a circular and symmetrical pattern (i.e. the perimeter of the droplet was approximately a circle). Due to the symmetry of the resulting circular droplet, which grows parallel to the medium surface, the droplet was modeled with 2-dimensional analysis. Figure 4 shows a 2-dimensional mesh plot. It was generated using the commercial software package Gambit. The nozzle and air chamber of the mesh was composed of 4 node quadrilateral elements that had an

edge length of 0.125 mm. The medium section of the mesh was also created with quadrilateral elements, but with a much smaller edge length depending on the medium. Mesh independence was verified by refining the mesh and ensuring that the results were not significantly different. The mesh was refined by reducing the element edge length by half. This resulted in a 2% change in the resulting droplet geometry, and was not considered significantly different. The refined mesh significantly increase computation time, thus the coarser mesh was used.

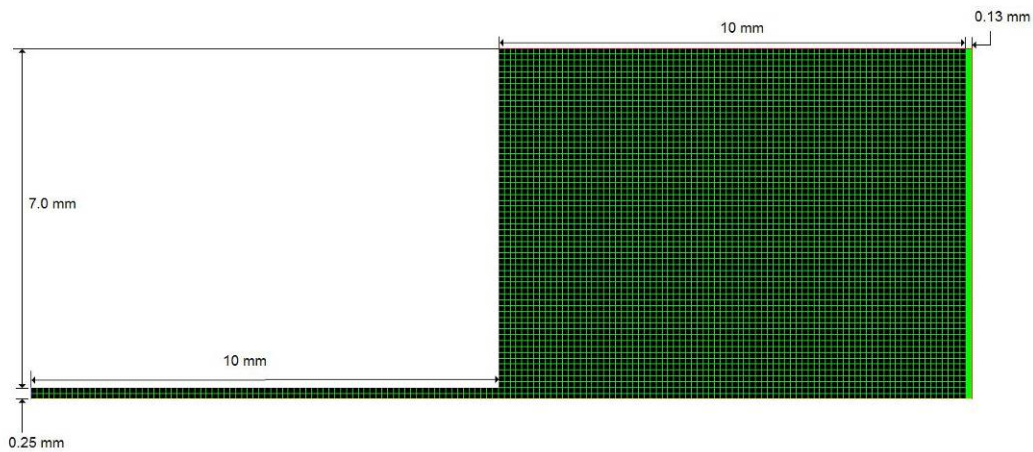


Figure 4: Typical Mesh Plot

In Fluent, an axisymmetric condition must be mirrored around the x-axis. Thus, the nozzle velocity and corresponding flow of the droplet were in the x-direction. Using the camera function in Fluent, the mesh was rotated clockwise by 90°.

### 3.3 Boundary Conditions

A velocity inlet was specified for the uppermost horizontal line of the model, while the lowermost horizontal line was specified to be a pressure outlet boundary

condition (Figure 2). A pressure outlet boundary condition was also specified along the vertical lines of the air chamber and medium.

The line between the air chamber and porous medium was specified as an interior boundary. This represents the boundary between the porous and non-porous fluid zones. The porous zone represents the porous medium and creates resistance to fluid flow through the zone.

The remaining lines/boundaries were specified as walls. This created two different wall conditions: the nozzle wall and the air chamber wall. A contact angle between the fluid mixture and the walls of the syringe nozzle was defined as 90 degrees, which represents the contact angle between water and steel. The nozzle was assumed to be composed of steel.

### **3.4 Fluent Models**

The volume of fluid (VOF) model within Fluent was used to define the droplet model. The VOF model assumes a multi-flow problem. In this case the two fluids are water and air. Several options are available within the Fluent VOF model to determine the droplet's geometry at the air/water interface. For this model the "Geometric Reconstruction Scheme" was used. The geometric reconstruction scheme interpolates near the interface of the two fluids using the piecewise-linear approach shown in Fluent User's Guide [2007].

Air was defined as the primary phase with water considered as the secondary phase. The two phases together are referred to as the fluid mixture. Fluent uses the continuum surface force (CSF) model for surface tension. The CSF model adds an additional source term to the momentum equation. This source term represents a pressure drop across the surface between the two fluids. The pressure drop is a function of the surface tension coefficient. Wall adhesion was also enabled within the Fluent model.

The wall adhesion represents the contact angle between the fluid and wall. Contact angle is related to the surface tension at the wall/fluid interface.

In addition to the VOF model, Fluent's porous medium model was also enabled for the "porous zone" of the model. Applying the porous medium model to a fluid zone, results in a pressure loss for the flow. The model takes into account a viscous and inertial loss term. The viscous and inertial resistance coefficients and direction must be determined and set within the Fluent model. For a 2-dimensional mesh, one direction vector for the coefficients was required. This model assumed the porous zone that simulates paper to be anisotropic, thus the resistance coefficients differed in the two directions. The porosity of the medium also needed to be specified.

For a porous medium, the flow is considered laminar if the Reynolds number is less than 1, as described in Perry and Green [1997]. The Reynolds number is defined as:

$$\text{Re} = \frac{D_x \rho v_{imp}}{\mu} \quad (1)$$

The fiber, or particle, diameter will be very small (~0.01 mm or less). Inserting the small fiber diameter into equation 1 along with the density and viscosity values for water, it can be seen that the impact velocity, must be less than 0.1 m/s in order for the flow to be considered laminar. This is a very small velocity, especially considering the droplet is ejected from a nozzle. Thus, the flow was assumed to be turbulent. Fluent has a few different models available for turbulent flow conditions. The  $\kappa$ - $\omega$  model will be used for the droplet model. This model is based on the Wilcox [1993]  $\kappa$ - $\omega$  model, which can be applied to low-Reynolds-number models. For the  $\kappa$ - $\omega$  model, Fluent uses the Reynolds-averaged approach to calculate time-dependent solutions of the Navier-Stokes equations, as presented in Fluent User's Guide [2007].

### 3.5 Fluent Solver

After defining the model for the droplet, the flow solver with Fluent was used to numerically solve the model. Fluent has the ability to solve flow problems using either a pressure or density based solver. Both the pressure and density-based solvers are able to solve the governing flow equations for a model by discretizing the geometry and integrating the conservation of mass and momentum equations. The geometry is discretized using the finite volume approach. The two different flow solvers differ in how they linearize and solve the discretized equations.

For the droplet model the pressure-based solver was used, as the density-based solver cannot be used with the VOF model. The pressure-based solver determines the pressure field for the flow by solving a pressure equation, which was created by manipulating the governing equations. These manipulated governing equations for continuity and momentum are numerically solved using the projection method. The projection method uses a pressure correction equation to ensure that the velocity field satisfies the continuity equation. For the droplet model the continuity and momentum equations were solved sequentially using the segregated algorithm. Second-order accuracy was specified for the equations since a quadrilateral mesh was used for the model. This was done by setting the momentum scalar equation to “QUICK” in Fluent’s solution controls panel. The QUICK scheme is appropriate for quadrilateral meshes. The pressure interpolation scheme was set to the “PRESTO!” scheme, which is recommended for flows involving porous medium. For “Pressure-Velocity Coupling”, the PISO algorithm was used. The PISO algorithm is recommended for all transient flow calculations. The non-iterative time advancement scheme was used to cut down on computational time by reducing the iterations performed for each time-step while preserving the overall accuracy of the results.

The droplet model needs to be solved for different time intervals, and thus the model was solved as a transient problem. This means that the governing equations had to be discretized for both time and space. For the droplet model, a fixed time step was



specified. During the discretization process, all time dependent equations were integrated over the fixed time step.

### 3.6 Input Data

The models within Fluent require a few important parameters to be defined. Within the VOF model a surface tension coefficient for the porous substrate and fluid was specified. The methods used to determine the surface tension coefficient and other input variables described in this section are given in the next section.

The porous medium model within Fluent requires two coefficients to be defined by the user. Those coefficients are related to the viscous and inertial forces applied by the fluid. The porous medium model adds an additional source term to the momentum equations, i.e., the Navier-Stokes equations. This source term creates a momentum sink that contributes to the pressure gradient within the porous medium. For the case of the droplet model, the paper will be considered as a homogeneous medium. The source term ( $S_i$ ) for a homogenous porous medium, as stated in Fluent User's Guide [2007], is defined as:

$$S_i = -\left(\frac{\mu}{\alpha} v_i + C_2 \frac{1}{2} \rho v_m v_i\right) \quad (2)$$

As seen in equation 2, the source term is composed of two parts. The first part accounts for viscous effects and is represented by Darcy's equation. The second term accounts for inertial losses, and the coefficient  $C_2$  represents the inertial resistance coefficient.

Another coefficient is defined to account for viscous effects. The viscous resistance coefficient (VR) is related to the medium's permeability ( $\alpha$ ) through the following equation:

$$VR = \frac{1}{\alpha} \quad (3)$$

In addition to the porous medium and VOF model, an impulse velocity was applied at the nozzle inlet. The velocity was applied for specified time duration. When

modeling turbulent flow in Fluent, both the  $\kappa$  and  $\omega$  values at any inlet boundary must be defined. For the droplet model there is only one inlet boundary condition, which is at the nozzle inlet.

### 3.7 Property Calculations

The important properties associated with the droplet system needed to be defined within the Fluent model. These properties included porosity, permeability, and surface tension.

#### 3.7.1 Porosity and Permeability

The permeability, and thus the viscous resistance coefficient, was determined based on the fibrous and packed bed models. Tabulated experimental data for a cellulose fibrous mat was used to determine the permeability of uncoated medium. The experimental data was based on the work Nilsson and Stenstorm [1997], which compared the solid void fraction to the dimensionless permeability of the medium. The dimensionless permeability is defined by the following equation:

$$P = \frac{\alpha}{a^2} \quad (4)$$

Tabulated results for their experimental data of a random fiber arrangement are shown in Table 1.

Table 1: Tabulated Permeability Data for Cellulose Fibers by Nilsson and Stenstorm [1997]

$\phi$	P
0.3	0.0195
0.4	0.00633
0.5	0.00109

Figure 5 plots the data in Table 1 in order to create a best fit equation that was used to determine a media dimensionless permeability based on its solid void fraction. An exponential trend-line provided the best fit curve fit for the data points.

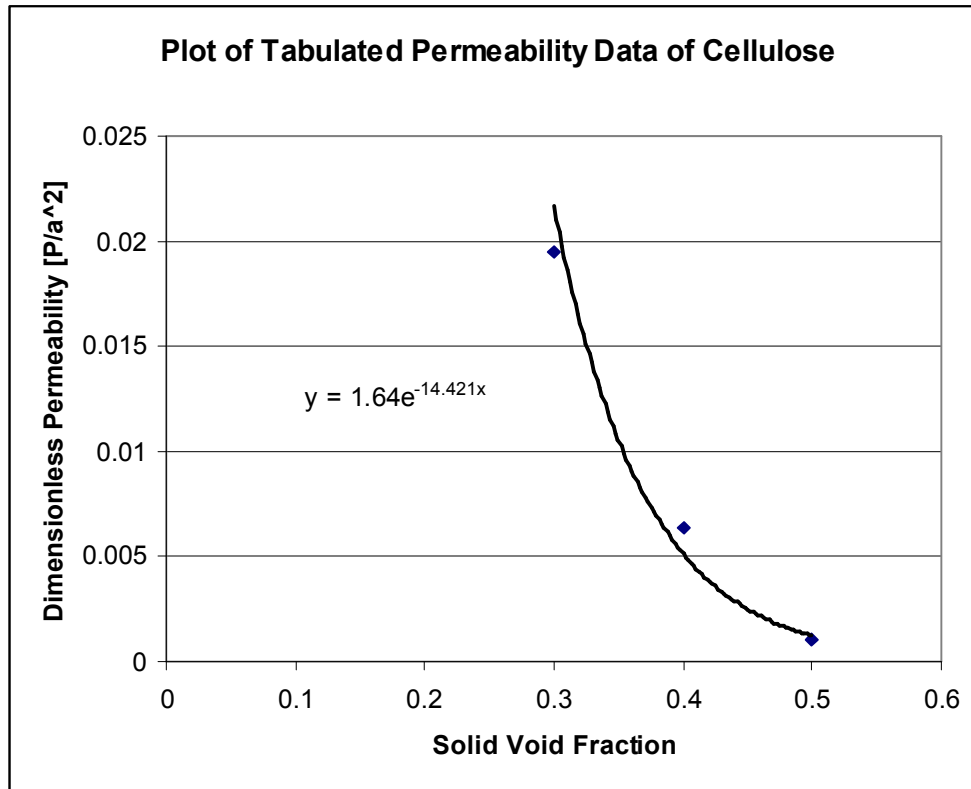


Figure 5: Plot of Tabulated Cellulose Permeability Data

The fiber diameter for a medium was measured using a high magnification microscope.

The total solid fraction for a medium can be defined by the following equation:

$$\phi = \frac{G}{L_m \rho_s} \quad (5)$$

Dry cellulose is considered to have a density of 1.61 g/cm<sup>3</sup> based on the work of Campbell [1947]. It is important to note that cellulose fibers can also absorb water themselves, but for this study it was assumed that the basis weight was measured for

“dry” sheets. The basis weight is usually specified on the ream label, and in general water accounts for 3-6% of the basis weight.

An alternative to using the basis weight is to use the dry weight of the medium to calculate the solid fraction.

$$\phi = \frac{W_{dry}}{L_m A_s \rho_s} \quad (6)$$

The dry weight of the sample was measured with a moisture balance, which is a scale with a heat controlled surface. A sample was placed on the scale and then heated until most of the water had been evaporated from the medium. As the water evaporated the weight of the medium and scale continued to change with time until most of the water had evaporated off when the weight of the medium reached steady state. The weight reported by the scale at steady state was used as the dry weight. Overall thickness of the medium was measured with the help of a microscope.

Either equation 5 or 6 can be used to calculate the solid volume fraction for the medium. Equation 6 should be more accurate since it ensures that all moisture has been removed from the medium, and it was used for un-coated plain paper. Once the solid fraction was calculated it was compared with previous experimental data to determine the appropriate dimensionless permeability number. The dimensionless permeability and measured fiber diameter along with equation 4 to determine the medium’s permeability.

Coated paper typically has two distinct porous layers: the base and the coating layer. The solid fraction has to be calculated separately for each layer. Since it would be quite difficult to physically separate the layers and determine the dry weight using the moisture balance, equation 5 was used to calculate the solid fraction for coated media.

The base layer of a coated medium is typically composed of cellulose fiber, like those found in plain paper, but the coated layer is usually composed of tiny pigment/polymer particles. The medium is commonly coated on two sides, with the base

layer sandwiched between the coating layers. Inkjet media require a porous coating layer that can absorb the ink. For these media, the coating layer is commonly composed of a silica base. In general, the silica particles have a diameter of  $\sim 0.1 \mu\text{m}$ .

A microscope was used to determine the thickness of the coating layer. The overall thickness of the coated medium was also measured and used to determine the base layer thickness. The coating thickness is calculated by subtracting the thickness of the base layer from the total thickness and then dividing by the number of coating layers,  $n$ .

$$L_c = \frac{L_m - L_B}{n} \quad (7)$$

The fibrous matte method used for determining the permeability of an uncoated medium was also applied to the base layer of a coated medium.

The void fraction and solid fraction are related to each other through the following relationship:

$$\varepsilon = 1 - \phi \quad (8)$$

Once the void fraction of the coating layer was determined, the permeability of the coating layer was determined using relationships derived for a packed bed.

From Ergun's [1952] work with packed beds, the permeability and inertial resistance coefficient can be defined as the equations given in Fluent user's guide [2007]:

$$\alpha = \frac{D_x^2 \varepsilon^3}{150(1 - \varepsilon)^2} \quad (9)$$

$$C_2 = \frac{3.5(1 - \varepsilon)}{D_x \varepsilon^3} \quad (10)$$

Once the permeability of the coated or uncoated medium was determined, equation 3 was used to calculate the viscous inertial coefficient of the medium, and inputted into Fluent's porous medium model. The porosity, or void fraction, was also required to be specified within the porous substrate model.

For turbulent flow within the porous region, both the viscous and inertial resistance coefficients must be defined. Equation 10 was used to determine the inertial resistance coefficient for a coated medium. For an uncoated medium, the inertial resistance coefficient can be found using the equations for flow through a perforated plate with an adjusted loss factor,  $K_L'$ , which is described in Fluent user's guide [2007]. An inertial resistance coefficient,  $C_2$ , for the plate is defined as:

$$C_2 = \frac{K_L'}{L_m} \left( \frac{1}{\varepsilon} \right)^2 \quad (11)$$

The procedure that was used to arrive at this equation is shown in Appendix A. Equation 11 was used to determine the inertial resistance coefficient for an uncoated medium. The loss factor at the inlet of the porous region can be treated as a sharp-edged entrance. For flow at a sharp-edged inlet, the loss factor is 0.5 as stated by Young et al. [1997].

### 3.7.2 Anisotropic Permeability

Within Fluent's porous medium model the permeability of the medium can be specified for 2-3 different directions. The transverse direction is referred to as direction-1 within the porous model, while the in-plane direction is referred to as direction-2, as shown in Figure 6.

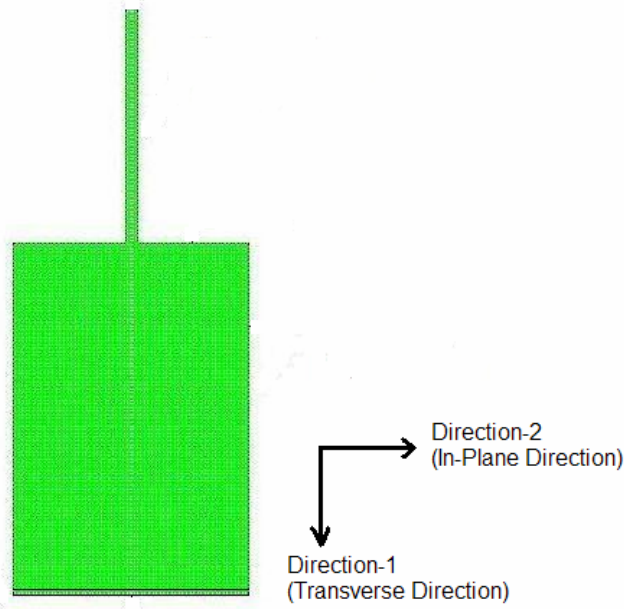


Figure 6: Permeability Direction Vectors in Fluent Model

For the 2-dimensional droplet model, both the in-plane and transverse permeabilities are specified. Based on the work of Hamlen and Scriven [1991], an anisotropic ratio of 5.5 was used to determine the in-plane permeability based upon the calculated transverse permeability.

### 3.7.3 Surface Tension

The surface tension was set with the VOF model. For the droplet system the three surface tension coefficients can be related to the contact angle between the substrate and droplet through the Young-Dupre relation given by De Gennes et al. [2004]:

$$\sigma_{LA} \cos \theta = \sigma_{SA} - \sigma_{SL} \quad (12)$$

For the droplet model the important surface tension coefficient is the substrate/liquid interface. This is the surface tension that was specified within the VOF model. The surface tension coefficient of the liquid/air interface can be determined from tabulated data for air and water. As mentioned previously, surface tension can be related to the

Van der Waals energy as shown by De Gennes et al. [2004]. Using this relationship, the following equation was derived for the surface tension at the substrate/air interface:

$$\sigma_{SA} = \frac{\sigma_{LA} (\cos \theta + 1)^2}{4} \quad (13)$$

The derivation of equation 13 is shown in Appendix B. Substituting equation 13 into equation 12, results in the following relationship:

$$\sigma_{SL} = \frac{\sigma_{LA} (\cos \theta + 1)^2}{4} - \sigma_{LA} \cos \theta \quad (14)$$

This was the equation used to compute the surface tension coefficient between the water droplet and porous medium.

### 3.8 Droplet Velocity

In the CFD model the droplet is subjected to an initial velocity,  $v_o$ , from the flow out of the syringe. After ejection from syringe, the droplet accelerates due to gravity. In order to match the desired droplet velocity at impact, the initial velocity of the droplet at the syringe was calculated based on the impact velocity from the experimental data and the following equation given by Meriam and Kraige [1997]:

$$v_o = v_{imp} - a_g t_d \quad (15)$$

The calculated initial velocity was applied at the syringe inlet of the CFD model

The  $\kappa$  and  $\omega$  values at the velocity inlet also had to be defined. These values were determined based on the following relationships stated in the Fluent User's Guide [2007]:

$$\kappa = \frac{3}{2} (v_o I)^2 \quad (16)$$

$$\omega = \frac{\kappa^{1/2}}{0.09^{1/4} \ell} \quad (17)$$

The velocity of the fluid was known at the nozzle inlet and corresponded to the initial velocity,  $v_o$ . The turbulence intensity and length scale were calculated based upon the following equations presented in Fluent user's guide [2007]:



$$I = 0.16(\text{Re})^{-1/8} \quad (18)$$

$$\ell = 0.07L \quad (19)$$

For the nozzle inlet, L is equal to the diameter of the nozzle. Thus substituting the nozzle diameter,  $D_{pipe}$ , into equation 19 results in the following equation for the turbulence length scale:

$$\ell = 0.07D_{pipe} \quad (20)$$

The Reynolds number for flow at the nozzle inlet can be determined from the following equation:

$$\text{Re} = \frac{\rho v_o D_{pipe}}{\mu} \quad (21)$$

Using the equations defined above, the turbulent kinetic energy and length scale were calculated and inputted into the Fluent droplet model. Fluent automatically calculates the values of  $\kappa$  and  $\omega$  at any non-inlet boundaries.

### 3.9 Media

Four different media were tested. These media and their associated properties are listed in Table 2. Media M1 was the only coated media tested. It was composed of two coated layers with a base layer in between. The coating layers are identical and are referred to as M1a, while the properties of the base layer were identified as M1b. Uncoated plain papers made up the remaining media: M2, M3, and M4. Each of the uncoated media had a unique porosity, permeability, and other material property values.

Table 2: Media Set

Media Name	G [g/m <sup>2</sup> ]	Lm [mm]	$\Phi$	$\epsilon$	Dx [mm]	$\sigma_{SL}$ [dyn/cm]	C <sub>2</sub> [1/m]	$\alpha$ [m <sup>-2</sup> ]	VR [1/m <sup>2</sup> ]	
									Direction-1	Direction-2
M1a	15	0.0271	0.2083	0.7917	0.0010	2.56	1468745.33	7.63E-14	1.31E+13	2.38E+12
M1b	151	0.1361	0.6889	0.3111	0.0087	NA	37937.86	6.00E-15	1.67E+14	3.03E+13
M2	75	0.1277	0.4151	0.5849	0.0125	11.42	11441.56	6.46E-13	1.55E+12	2.81E+11
M3	75	0.1201	0.3769	0.6231	0.0104	7.04	10726.10	7.80E-13	1.28E+12	2.33E+11
M4	105	0.1430	0.4390	0.5610	0.0093	9.01	11107.67	2.50E-13	4.00E+12	7.27E+11

### 3.10 CFD Results

Results of the CFD modeling are presented in this chapter. The analysis and procedure for determining the input parameters for the model are also presented.

#### 3.10.1 Volume of Water within Media

The “Volume Integrals” function within Fluent was used to calculate the total volume of water within the porous medium zone. The volume integrals feature integrates over the specified cell or zone to determine the volume in that region. This was a useful feature within the CFD model that allowed the absorption of water by the medium to be tracked over time. Figure 7 shows the volume of water absorbed into three different uncoated media, specified as M2, M3, and M4, at various time intervals.

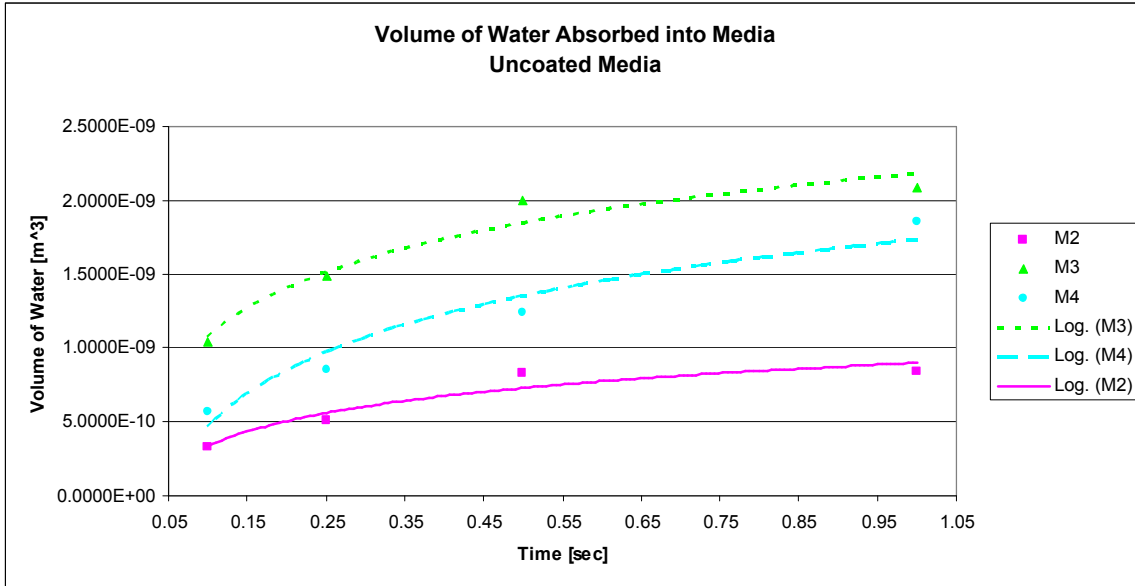


Figure 7: Volume of Water Absorbed from the CFD Model for Uncoated Media

The volume of water absorbed into the coated medium, specified as M1, was also plotted (Figure 8). The model was run for two different meshes: one mesh incorporated only the top coating layer (1-layer), and the other had three different layers made up of a base layer surrounded by two coating layers (3-layer). It shows that the 1-layer model/mesh results seem more reasonable since the 3-layer model has very little water absorption, which was an unexpected behavior since the coated medium considered was a porous coated medium that was known to be very absorptive. Also the results from the 1-layer model followed the same trend as the volume of water results for the uncoated models. This indicates that there were missing parameters or incorrect interface boundaries defined for the 3-layer model.

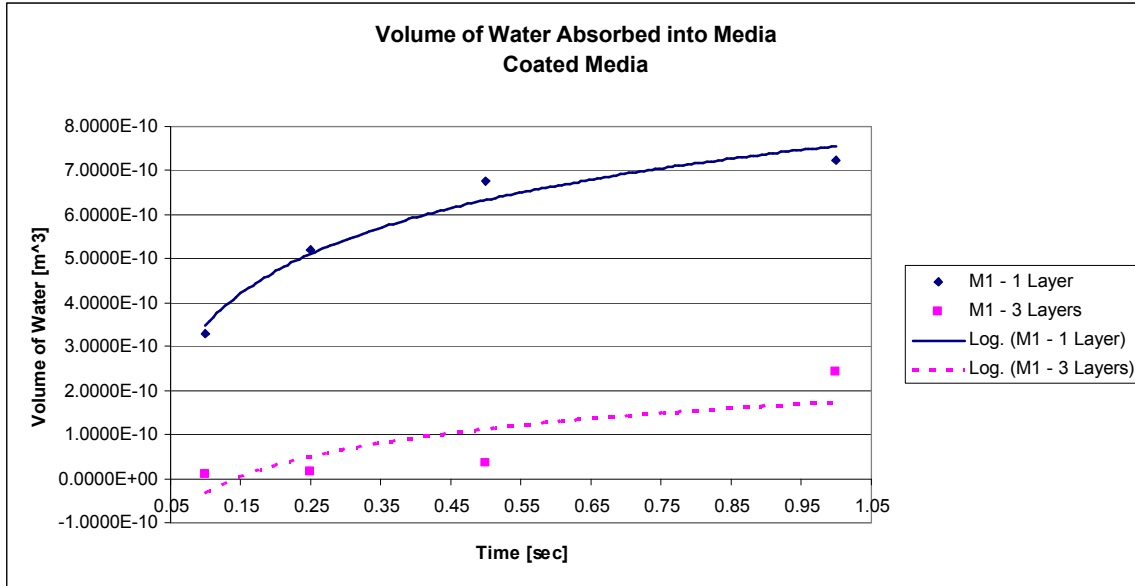


Figure 8: Volume of Water Absorbed from the CFD Model for Coated Media

### 3.10.2 Aspect Ratio

The resulting droplet shape after impact was characterized at various time intervals as the aspect ratio between the measured diameter and droplet height. The aspect ratio,  $r$ , was defined by the following relationship:

$$r = \frac{d}{h} \quad (22)$$

Figure 9 shows the resulting CFD aspect ratio for three uncoated media. The three media had different porosity, permabilities, and surface tension coefficients. All media had around the same drop velocity of 0.27 – 0.28 m/s

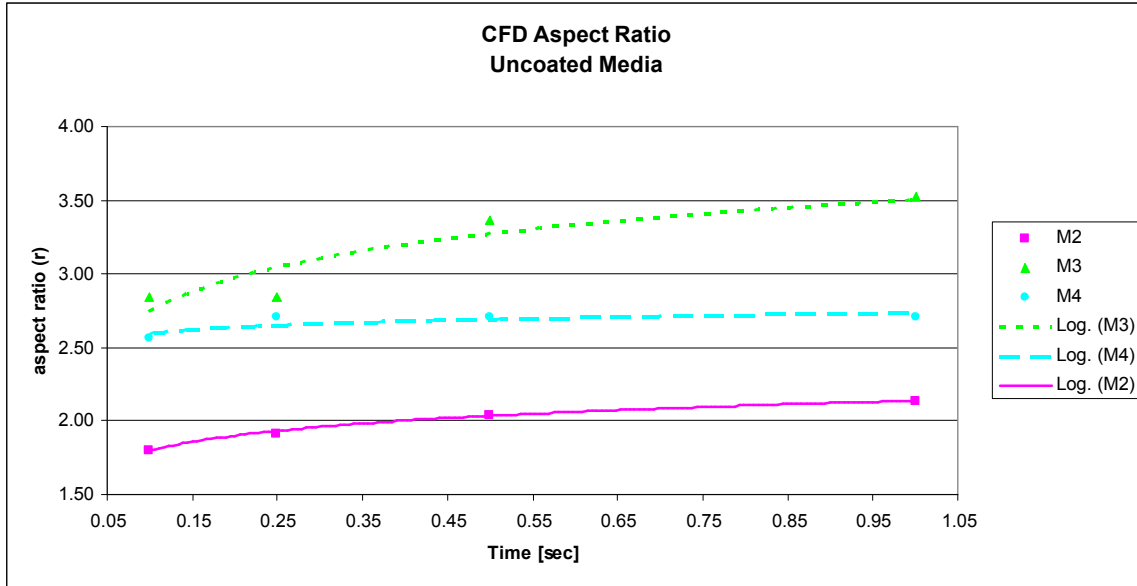


Figure 9: CFD Aspect Ratio for Uncoated Media

The coated medium was modeled with two different meshes: one with only 1-layer, the top coated layer, and another with 3-layers, which had two coated layers and a base layer. Results for the aspect ratio from the two different meshes are shown in Figure 10.

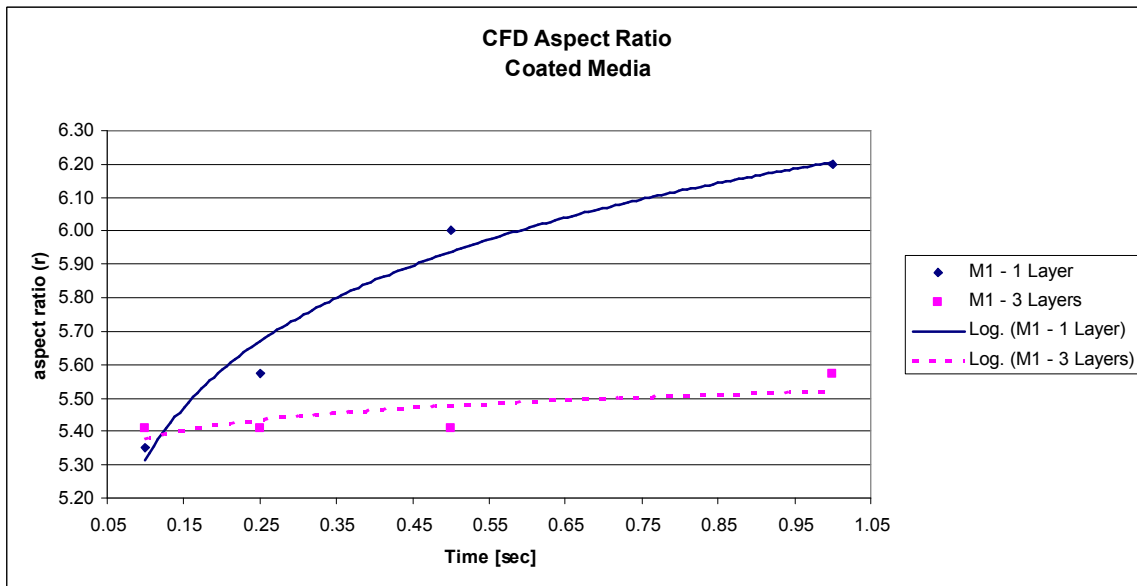


Figure 10: CFD Aspect Ratio for Coated Media

## **CHAPTER FOUR**

### **EXPERIMENTAL TEST FACILITY**

An experiment was set up with a high speed camera to capture images of a water droplet impacting with various porous media. The details of the equipment and procedure of the experiment are given in this chapter.

#### **4.1 Experimental Schematic**

Figure 11 shows a schematic of the experimental setup. The setup included a syringe that ejected a droplet onto a medium. The syringe and medium are attached to a common fixture. A high magnification scope lens was focused upon the syringe nozzle and medium. The lens was attached to a high speed camera. Figure 12 shows a picture of the fixture, nozzle, lens, and medium (paper). A computer attached to the camera recorded the video images of the droplet as it was ejected from the nozzle and impacted with the medium.

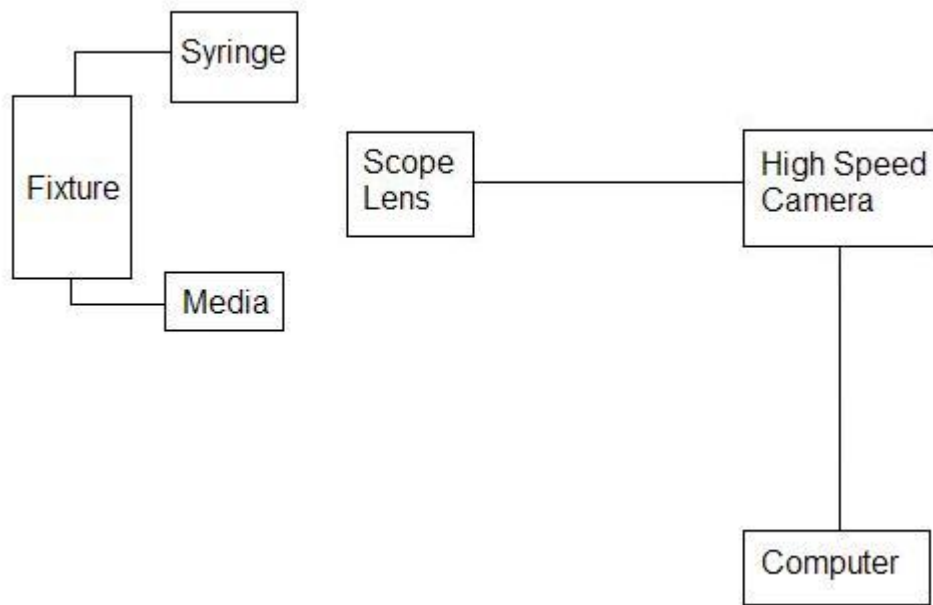


Figure 11: Experimental Schematic

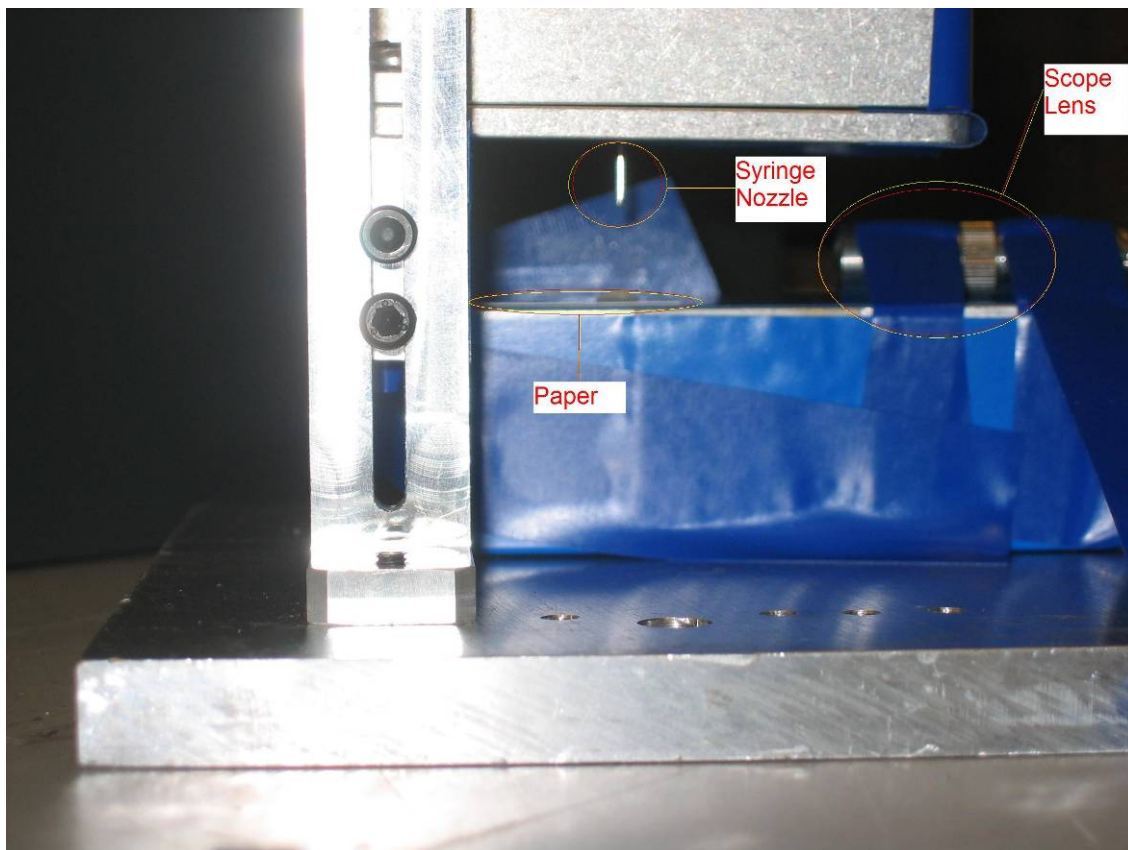


Figure 12: Close Up View of Syringe/Lens Setup

## **4.2 Syringe**

A syringe filled with de-ionized water was used to eject a water droplet. The syringe had a volume 10 mL. Attached to the end of the syringe was a nozzle with an inner diameter of 0.5 mm. The syringe was able to produce a single water droplet by temporarily compressing the syringe plunger by hand.

## **4.3 Fixture**

A fixture was used to position both the medium and syringe. The fixture was composed of a number of aluminum brackets. Using the brackets, the syringe was fixture such that the nozzle was perpendicular to the medium. The fixture was adjustable in the vertical direction and allowed the distance between syringe nozzle and medium to be adjusted. For the experiment the fixture was set to provide a 10 mm gap between the tip of the nozzle and the top of the medium.

## **4.4 Camera and Lens**

A high speed camera with a scope lens was used to record the droplet formation, ejection, and impact with the medium. The scope lens was able to fit into small spaces. For the experiment the lens was taped down to the fixture, and was able to provide a view of the end of the nozzle and medium, as shown in Figure 12. The camera was set to capture 400 frames per second, and the resulting video was saved at a playback rate of 1 frame per second. A total of 5.1 seconds of real time data was captured.

## **4.5 Other Equipment**

A moisture balance was used in order to calculate the solid fraction, and thus porosity of the media tested. The metal balance heats a sample up while in parallel measuring the weight of the sample. The resulting dry weight,  $W_{dry}$ , was used in



conjunction with equation 6 to determine the solid fraction of the medium. Samples of each of the uncoated media were tested. Each sample was a 60 by 60 mm square.

A microscope was used to measure the overall medium thickness, and for the uncoated media this was also used to measure the fiber diameter. The microscope had a camera attached, and a still image was captured for each measurement. Figure 13 shows a typical image used for measuring the overall medium thickness. For each medium, five different measurements were taken, and the average of those measurements was used as the overall medium thickness. The coating thickness was measured using the same procedure. Figure 14 shows one of the images used to determine coating thickness.

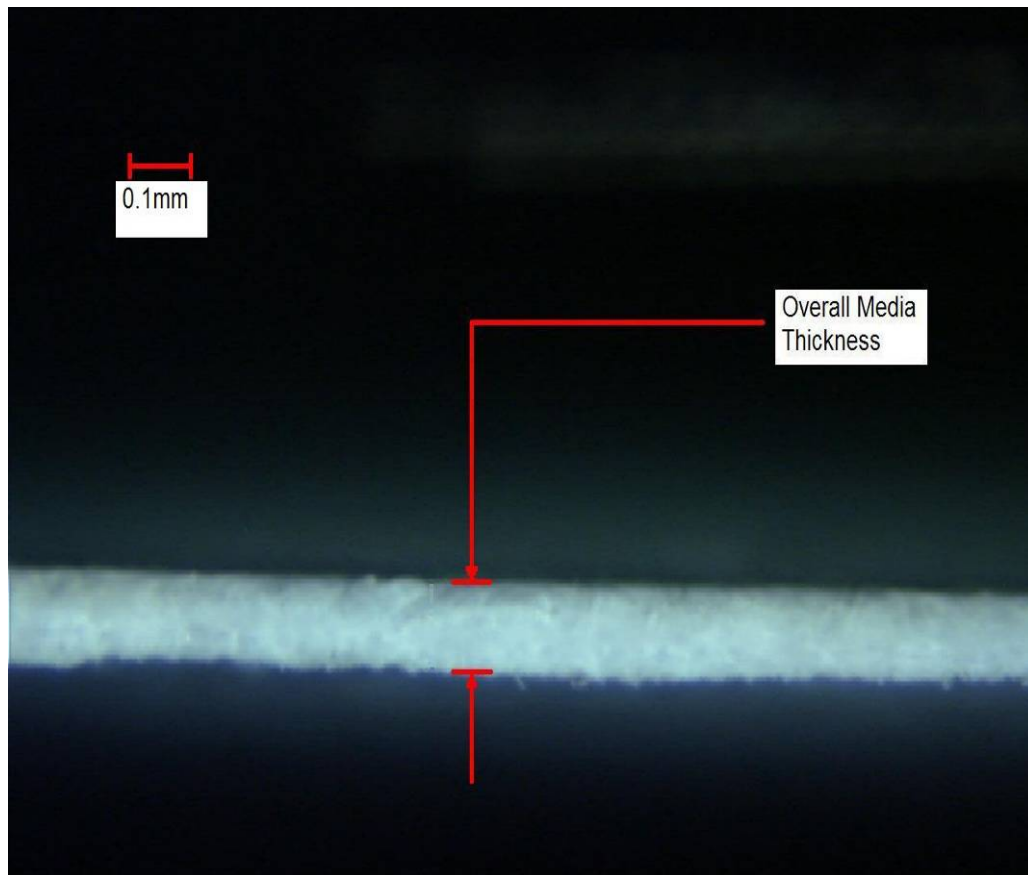


Figure 13: Media Thickness Image of M2

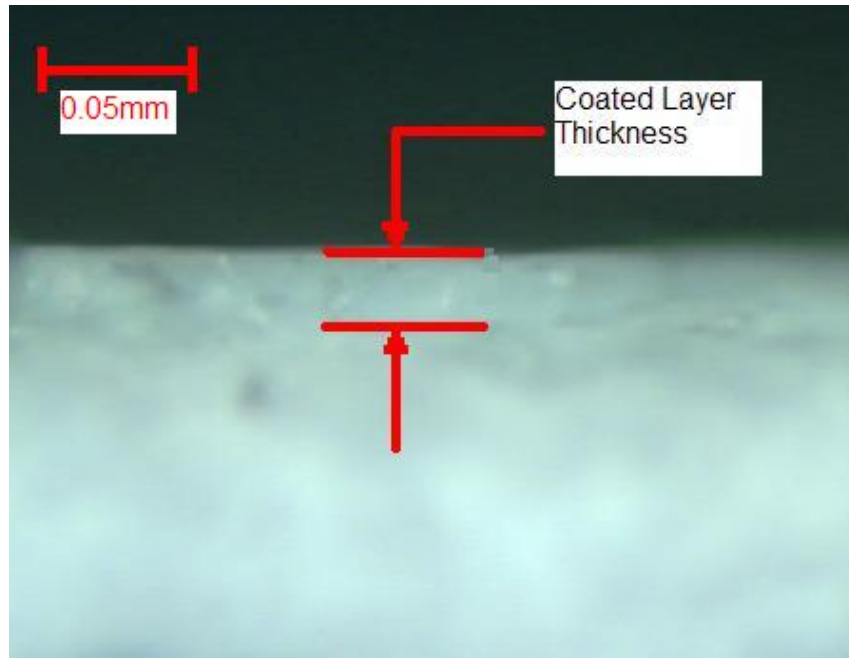


Figure 14: Coating Thickness Image of M1

Microscope images were also used to measure the fiber diameters of the uncoated media. Again five different measurements were taken for each medium, and the average was used as the fiber diameter of the medium. Figure 15 shows an example of a microscope measurement for fiber diameter.

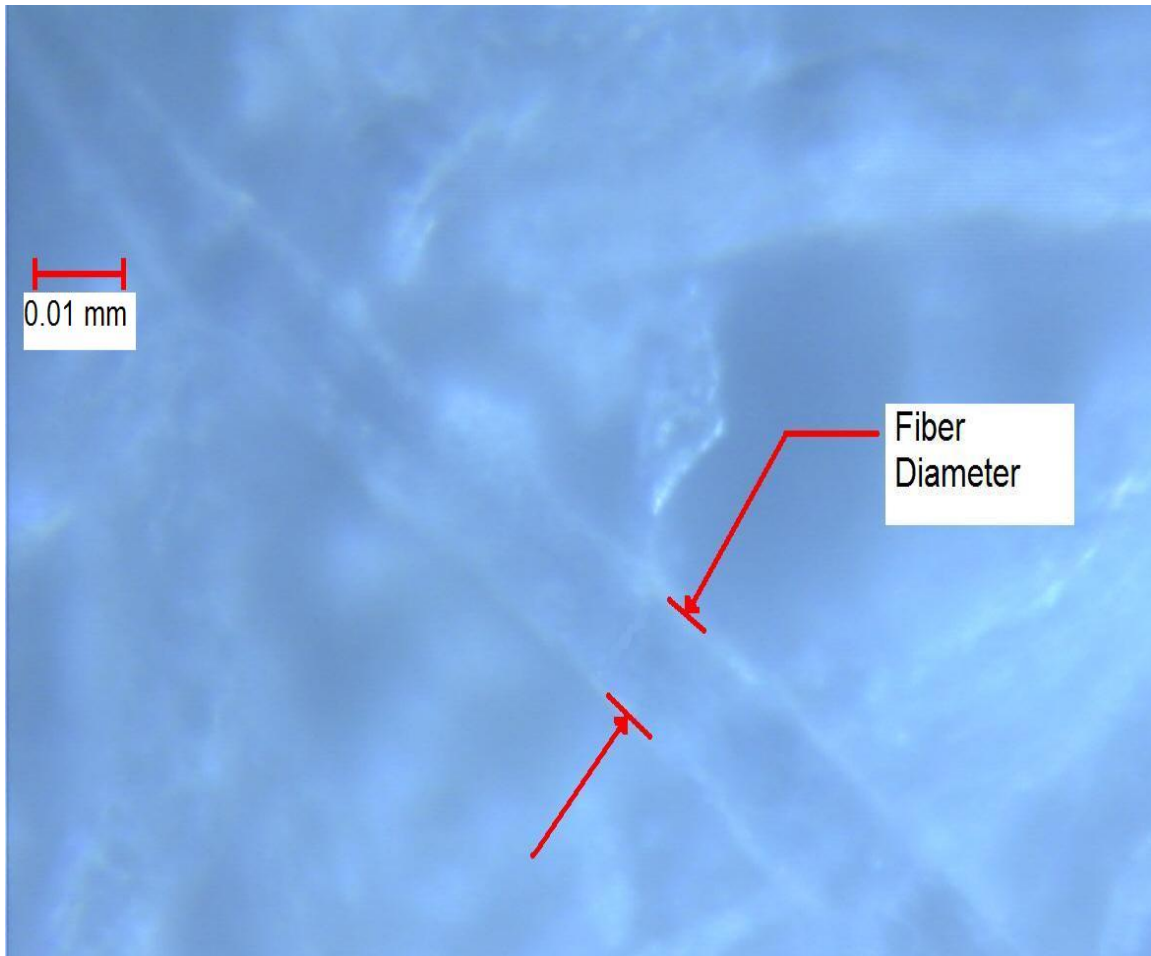


Figure 15: Fiber Diameter Image for M2

#### 4.6 Test Procedure

Water droplets impacting with various coated and uncoated papers were recorded with the high speed video camera. For each paper/medium, a sample was placed on a flat surface provided by the fixture. The syringe was then used to produce a water droplet that impacts with the medium. A high speed camera with a scope lens was used to record the droplet during ejection and impact with the paper. The camera captured video and still images of the droplet. These images were then analyzed to determine the droplet velocity and shape after it impacts with the medium.

This test procedure was repeated across the various media. The droplet volume and velocity were also varied across different experimental runs.

## CHAPTER FIVE

### EXPERIMENTAL RESULT AND COMPARISONS

Results from the experiment are presented in this chapter. The results for the aspect ratio are also compared with results from the CFD model.

#### 5.1 Calculated Properties

The images and video from the high speed camera was used to calculate properties associated with the droplet/medium system. These properties included the contact angle and average velocity.

##### 5.1.1 Contact Angle

The contact angle between the medium and water was measured from video images. Immediately after impact the droplet experiences an oscillating motion. Once this oscillation had dampened out, the contact angle was measured. The droplet was for the most part static at this point. Figure 16 shows a typical image of the contact angle. Four different measurements were taken for each medium, and the average of these four measurements used as the contact angle. Table 3 lists the resulting contact angle for each medium. The contact angle was then used, along with equation 14, to determine the surface tension coefficient between the medium and water droplet.

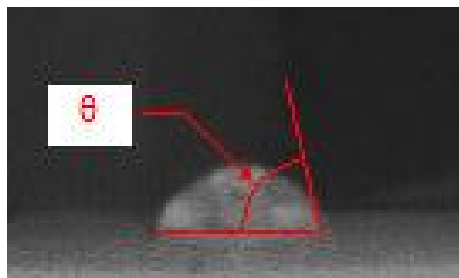


Figure 16: Contact Angle Image for M2

Table 3: Average Contact Angle

Media	Contact Angle [degrees]
M1a	51.5
M2	78.25
M3	68
M4	73

### 5.1.2 Average and Impact Velocity

Images from the high speed camera were analyzed to determine both the average and impact velocity of the droplet. The average velocity ( $V$ ) was determined by measuring the total height ( $H$ ) the droplet has fallen and the time it took to fall ( $t_d$ ), as shown in equation 23. The average velocity varied between runs in the range of 0.25 – 0.36 m/s.

$$V = \frac{H}{t_d} \quad (23)$$

A second velocity measurement was also taken to determine the impact velocity ( $v_{imp}$ ), which corresponds to the droplet's velocity right before impact with the medium. As the droplet approached a height of 2 mm above the medium, the exact distance between the droplet and medium was measured using the high speed camera images. This distance was specified as  $H'$ . The time it took the droplet to fall from  $H'$  to contact with the medium was also measured and recorded as  $t_d'$ . The following equation was then used to calculate the impact velocity, which varied from 0.25 - 0.42 m/s:

$$v_{imp} = \frac{H'}{t_d'} \quad (24)$$

For most of the experimental runs the initial droplet velocity out of the syringe was very small. The total height the drop had to fall,  $H$ , was also very small (~10 mm). Thus for cases with a small initial velocity, the impact velocity was approximately equal

to the average velocity. For a few cases, though, this was not the case, and the measured impact velocity was significantly higher than the average velocity measurement. Thus, the initial velocity out of the syringe was not negligible in these cases.

## 5.2 Aspect Ratio

The high speed camera images were also used to characterize the droplet shape after impacting with the porous medium. The droplet shape was characterized at various time intervals with the aspect ratio between the measured diameter and droplet height (Equation 22).

## 5.3 Data Comparisons

The aspect ratios from the CFD model were compared with those from the experimental data. The CFD versus experimental aspect ratio was plotted for each medium at a drop velocity around 0.27 - 0.28 m/s (Figures 17-20). It should be noted that the axes on the figures below do not start at zero.

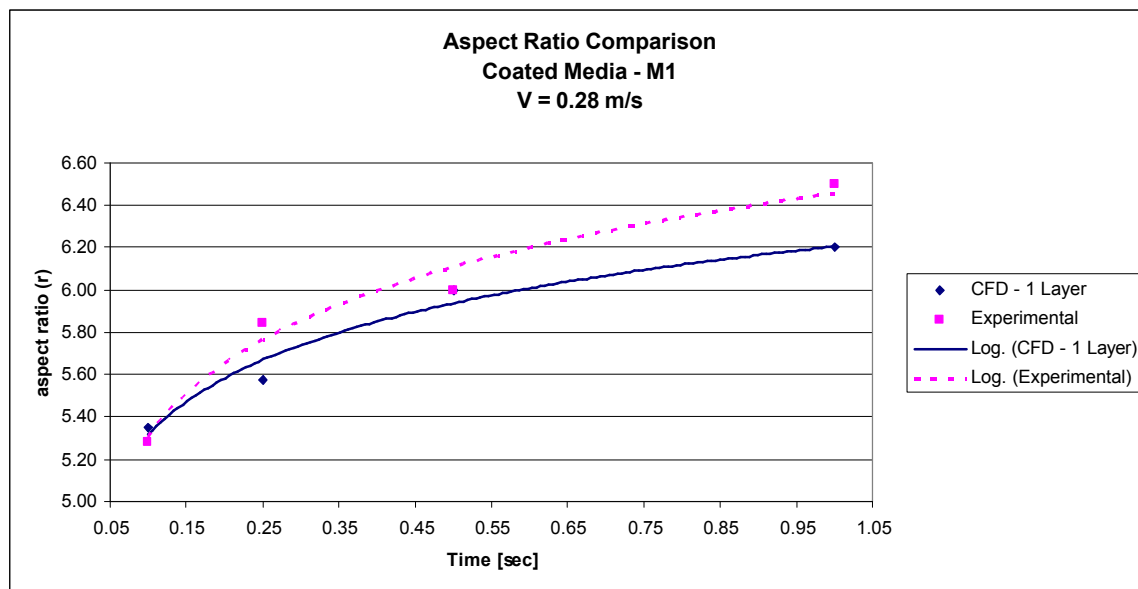


Figure 17: Aspect Ratio Comparison of M1

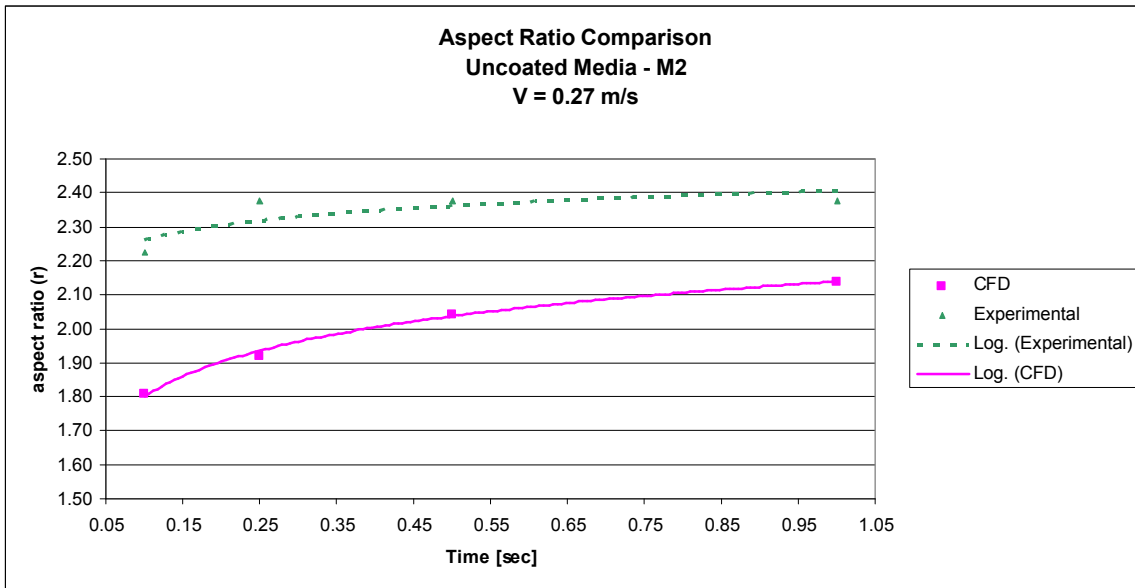


Figure 18: Aspect Ratio Comparison of M2

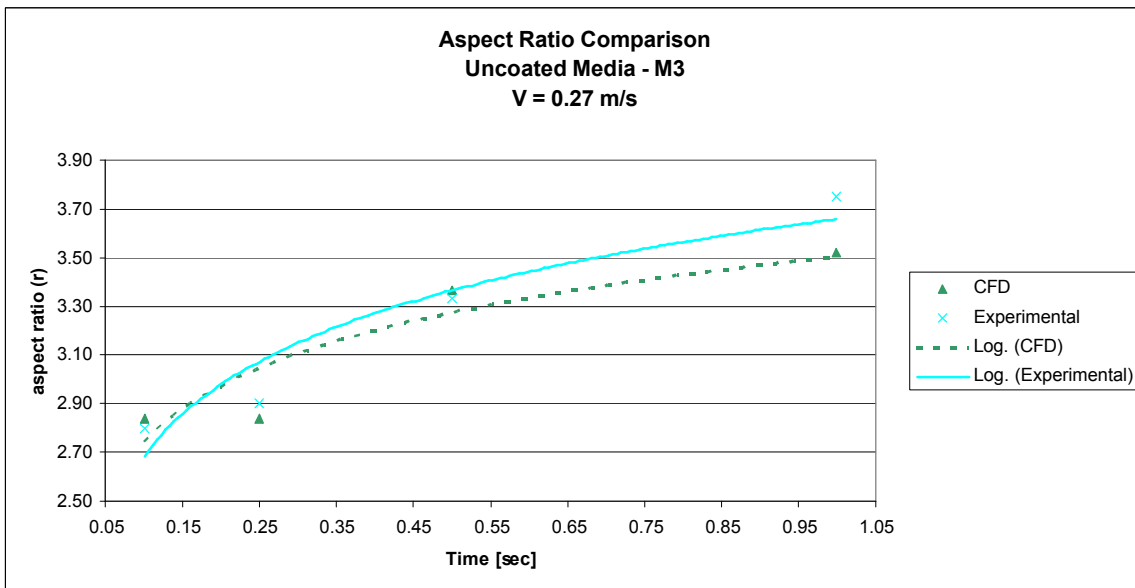


Figure 19: Aspect Ratio Comparison of M3

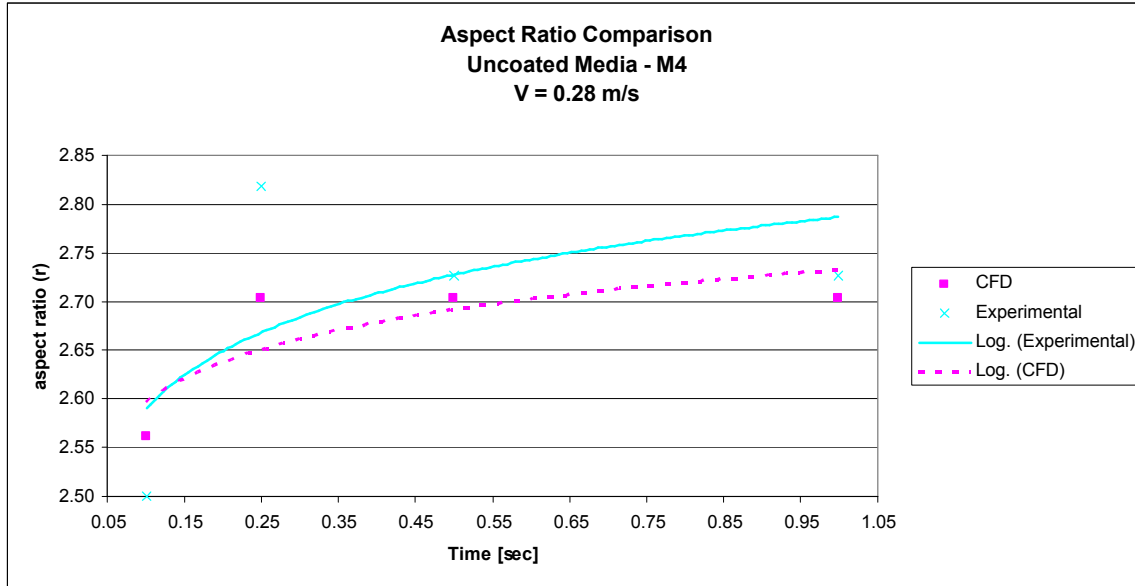


Figure 20: Aspect Ratio Comparison of M4

For each experimental run, a corresponding CFD model was also run. The aspect ratio was compared between each experimental and CFD run, and the associated deviation between the two was calculated. Figures 21 and 22 below show the percent deviation between the model and experiment aspect ratios. The following equation was used to calculate the percent deviation:

$$\%Deviation = 100 \left( \frac{r_{CFD} - r_{EXP}}{r_{EXP}} \right) \quad (25)$$



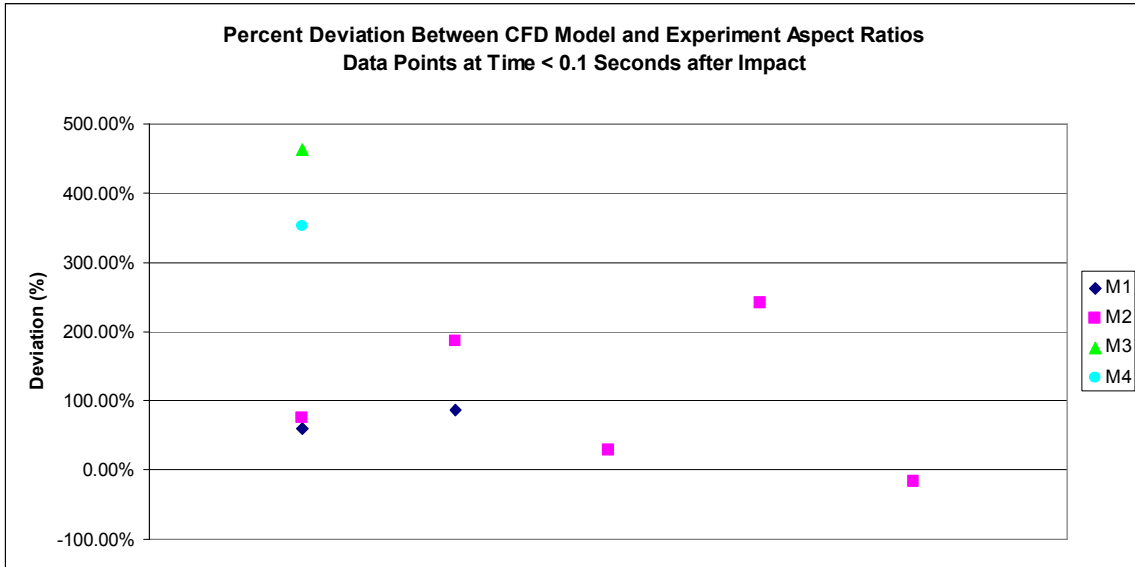


Figure 21: CFD Model Aspect Ratio Deviation < 0.1 Seconds after Impact

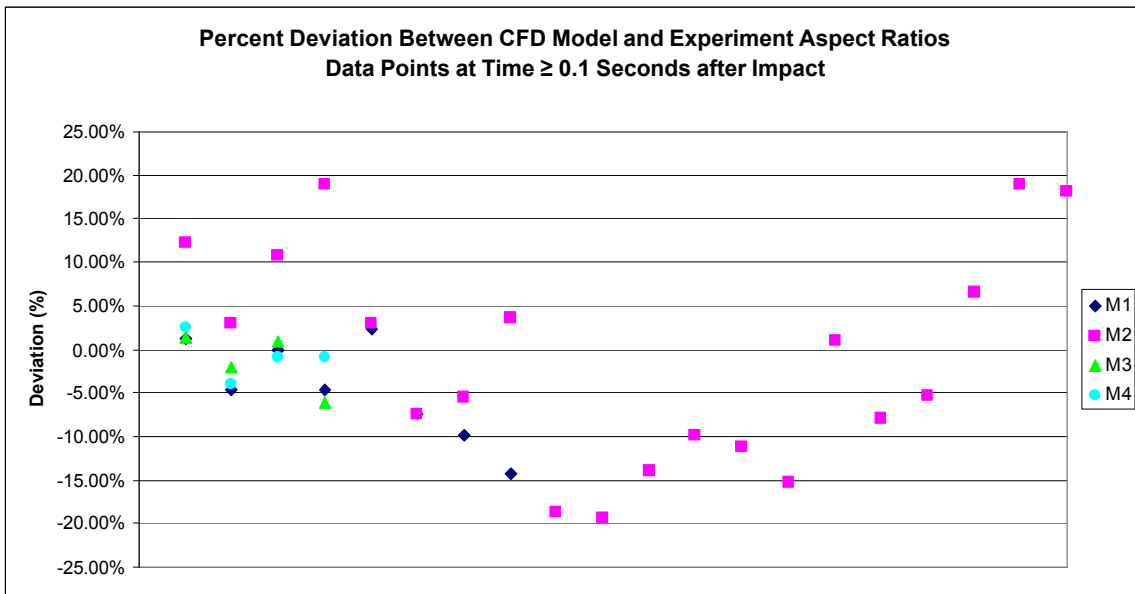


Figure 22: CFD Model Aspect Ratio Deviation ≥ 0.1 Seconds after Impact

The two figures above show that after a certain time, about 0.1 seconds after impact, the CFD model has an error range of +/- 20%. Yet the error associated with the predicted aspect ratio by the model increases significantly at times before 0.1 seconds. Images from the high speed camera show that immediately after impact, around 0.01

seconds, the droplet oscillates (Figures 24, 26, & 28). The CFD model lacks this oscillation effect (Figures 23, 25, & 27). By 0.1 seconds, the oscillation has subsided and the model more closely corresponds to the experimental results (Figures 29 & 30).

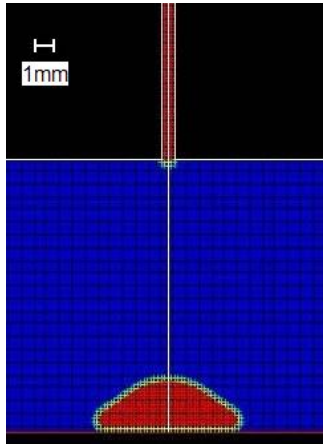


Figure 23: CFD at 0.005 sec.

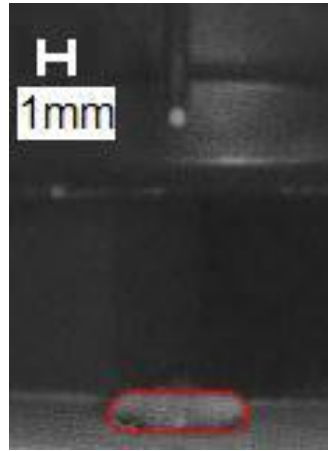


Figure 24: Experiment at 0.005 sec.

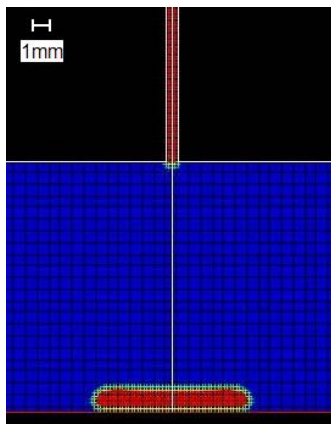


Figure 25: CFD at 0.01 sec.

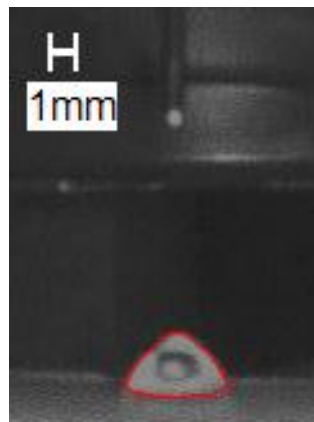


Figure 26: Experiment at 0.01 sec.

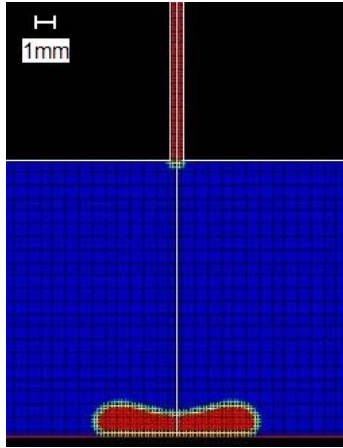


Figure 27: CFD at 0.02 sec.

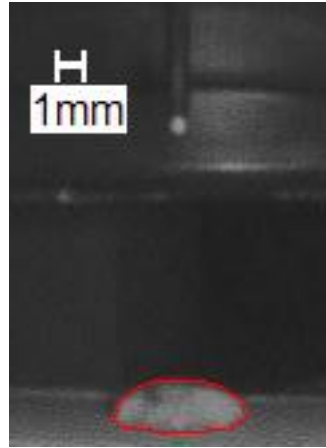


Figure 28: Experiment at 0.02 sec.

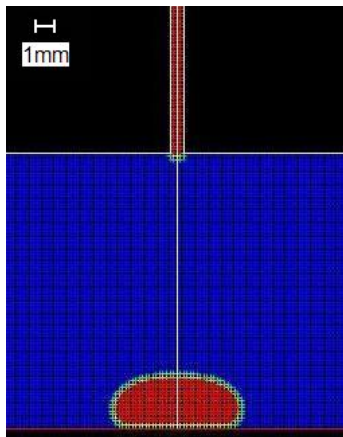


Figure 29: CFD at 0.1 sec.

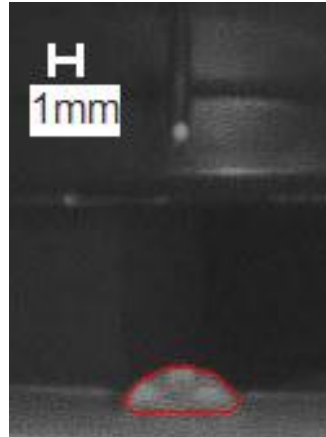


Figure 30: Experiment at 0.1 sec.

The results indicate that the porous medium model within Fluent is not able to account for all of the inertial effects that occur immediately after impact. It appears that the base porous model within Fluent is not able to account for all on the inertial forces produced at impact. The model does not treat the porous zone as a solid surface, but instead considers it another fluid zone that will have a pressure drop across it due to the porous zone. This could be a contributing factor to the lack of droplet oscillation immediately after impact. Thus the CFD model should only be used to predict the relative droplet geometry at a time interval greater than or equal to 0.1 seconds after impact.

## **CHAPTER SIX**

### **DIMENSIONAL AND UNCERTAINTY ANALYSIS**

A dimensional analysis was performed for the droplet/medium system. The analysis and results are presented in this chapter. An uncertainty analysis was also performed to determine the uncertainty associated with the parameters used in the CFD model and dimensional analysis. The procedure used to estimate uncertainty, along with the results is presented.

#### **6.1 Dimensional Analysis**

A dimensional analysis can be performed to help understand the physical parameters of a system and their relationship. The analysis produces a set of dimensionless equations that describe the important variables of the system. Since the equations are dimensionless they are independent of the system units, and thus could be applied to other systems. This also means that the dimensionless parameters are scalable. An application of the scalable feature would be to create a much smaller model of a system within a laboratory, where experimentation could easily occur. Any modeling of the system with non-dimensional variables could be applied to much large systems outside of the laboratory. This is an example of how a dimensional analysis can be used as an effective tool in understanding a system of variables.

The droplet system shown in figure 2 was subjected to a dimensional analysis. The Buckingham Pi theorem was used to determine the important non-dimensional terms required to describe the system. Using the non-dimensional variables, along with experimentation data, a function for the droplet's aspect ratio was derived. The dimensional analysis and results are presented in the next two sections.

### 6.1.1 Derive Pi Terms

A non dimensional analysis was performed for the droplet-medium interaction. Ten independent parameters were identified to be the important variables for the system under study through the following relationship:

$$f(h,d,H,D,V,\rho,\mu,\sigma,\varepsilon,t) = 0 \quad (26)$$

These variables consist of three basic dimensions; mass (M), length (L), and time (T). Upon inspection, three different repeating variables were identified. These three variables were:  $D$ ,  $V$ ,  $\mu$ .

With ten total variables and three repeating variables, seven non dimensional pi terms are required for the droplet system. These pi terms were calculated and these calculations can be found in Appendix C. The resulting pi terms are list below:

$$\pi_1 = \frac{h}{D} \quad (27)$$

$$\pi_2 = \frac{d}{h} \quad (28)$$

$$\pi_3 = \frac{H}{D} \quad (29)$$

$$\pi_4 = \frac{\rho V D}{\mu} = \text{Re} \quad (30)$$

$$\pi_5 = \frac{\rho V^2 D}{\sigma} = \text{We} \quad (31)$$

$$\pi_6 = \varepsilon \quad (32)$$

$$\pi_7 = \frac{tV}{H} = \tau \quad (33)$$

The fourth pi term resulted in the Reynolds number (Re), while the fifth pi term resulted in the Weber number (We). Also the second pi term was equal to the aspect ratio,  $r$ .

### 6.1.2 Aspect Ratio Correlation

Once the pi terms for the droplet system had been identified, they were calculated using the experimentation data. These pi terms were calculated for various media, drop velocities, drop volumes, and time intervals. Each medium had a different porosity, or

void fraction, along with a different surface tension between the medium and fluid.

Figures 31 and 32 show some of the results.

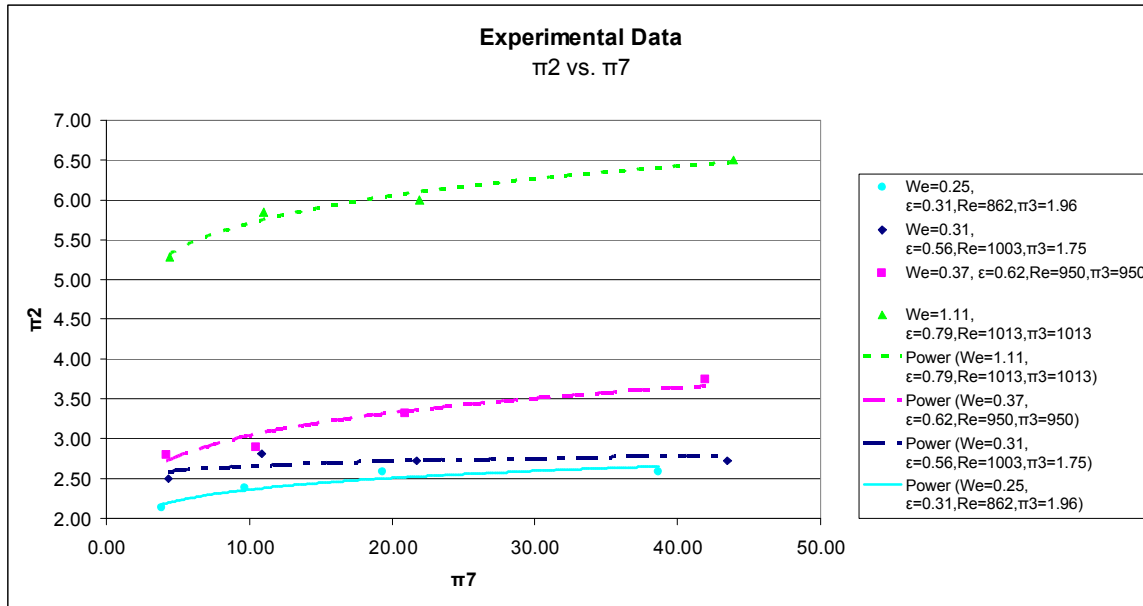


Figure 31:  $\pi_2$  versus  $\pi_7$  for Various Weber Numbers and Porosities

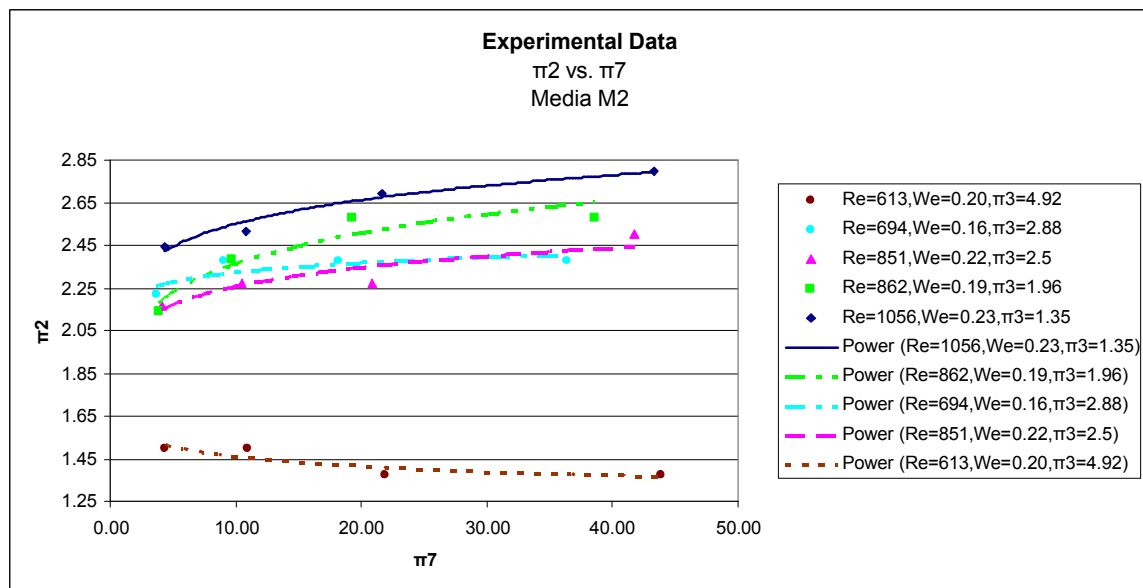


Figure 32:  $\pi_2$  versus  $\pi_7$  for Various Reynolds Numbers

Figure 31 shows that as the surface tension between the fluid and medium decreases, the droplet aspect ratio increases. The aspect ratio also increased as the porosity increased. There was also a small increase in the droplet aspect ratio over time. For most cases as the Reynolds number increased, the aspect ratio also increases, as shown in Figure 32. Not all cases fit this trend, though, and it should be noted that the drop volume was different between each run. The highest drop volume corresponded to the lowest aspect ratio. Thus the variation in drop volume may contribute to the deviations in a clear trend between the Reynolds number and aspect ratio.

Since the entire seven pi terms were varied across the different experimental runs and medium combinations, a relationship was derived between the aspect ratio,  $\pi_2$ , and the remaining six pi terms. It was assumed that the aspect ratio was a function of the remaining pi terms, as shown in the equation below.

$$\pi_2 = C\pi_1^{a1}\pi_3^{a3}\pi_4^{a4}\pi_5^{a5}\pi_6^{a6}\pi_7^{a7} \quad (34)$$

A system equation was developed by rearranging equation 34 such that one side of the equation was equal to zero. The resulting system equation,  $f_i$ , is shown below.

$$f_i = \frac{C\pi_1^{a1}\pi_3^{a3}\pi_4^{a4}\pi_5^{a5}\pi_6^{a6}\pi_7^{a7}}{\pi_2} - 1 = 0 \quad (35)$$

The pi terms calculated for each experimental run were used to develop a set of system equations. Using the ‘‘Solver’’ feature within Excel, the unknown coefficients were then determined based on the set of system equations. The Solver feature was set up to minimize the sum of the squares of the system equations. The sum of the squares is defined by the following relationship:

$$\sum_{i=1}^m \left( f_i - \bar{f} \right)^2 \quad (36)$$

The mean value,  $\bar{f}$ , was zero for the system equation, as defined by equation 35. Excel’s Solver feature determined the coefficient values that would minimize the sum of

the squares of the system equations based on the experimental data. Appendix D shows the Solver worksheet. The resulting equation is shown below:

$$\pi_2 = 0.328\pi_1^{-1.56}\pi_3^{-0.0861}\pi_4^{0.1395}\pi_5^{-0.0506}\pi_6^{0.0302}\pi_7^{-0.0277} \quad (37)$$

Equation 37 has a percent deviation of +/- 10% from the experimental aspect ratio for data points at a time greater than or equal to 0.1 seconds after impact (Figure 33).

The standard deviation for the range is 2.72%. The equation is only valid for the following parameter intervals:

$$613 \leq Re \leq 1056$$

$$0.16 \leq We \leq 1.11$$

$$0.31 \leq \varepsilon \leq 0.79$$

$$3.87 \leq \tau \leq 43.45$$

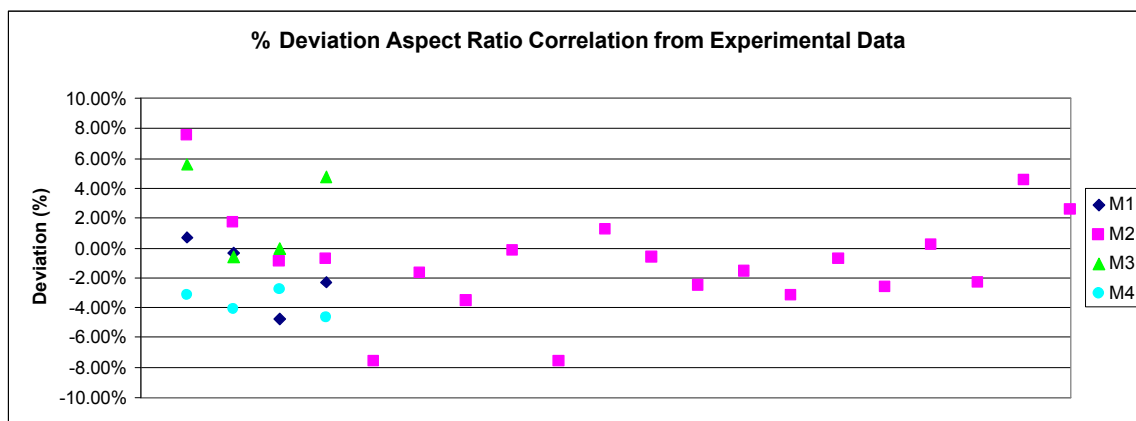


Figure 33: Percent Deviation of Aspect Ratio Correlation

## 6.2 Uncertainty Analysis

The uncertainty analysis was carried out to calculate the uncertainty associated with the aspect ratio correlation. The uncertainty was also calculated for all major input parameters into the CFD model.

Equation 37 for the aspect ratio has seven parameters associated with it, as shown below:



$$\pi_2 = 0.328 \frac{D^{1.735} \rho^{0.0889} V^{0.0106} \sigma^{0.0506} \varepsilon^{0.0302}}{h^{1.56} H^{0.0584} \mu^{0.1395} t^{0.0277}} \quad (38)$$

The uncertainty associated with the aspect ratio equation,  $U\pi_2$ , was calculated using the following relationship:

$$U\pi_2 = \frac{1}{\pi_2} \left( \left( \frac{\partial \pi_2}{\partial D} U_D D \right)^2 + \left( \frac{\partial \pi_2}{\partial \rho} U_\rho \rho \right)^2 + \left( \frac{\partial \pi_2}{\partial V} U_V V \right)^2 + \left( \frac{\partial \pi_2}{\partial \sigma} U_\sigma \sigma \right)^2 + \left( \frac{\partial \pi_2}{\partial \varepsilon} U_\varepsilon \varepsilon \right)^2 + \left( \frac{\partial \pi_2}{\partial h} U_h h \right)^2 + \left( \frac{\partial \pi_2}{\partial H} U_H H \right)^2 + \left( \frac{\partial \pi_2}{\partial \mu} U_\mu \mu \right)^2 + \left( \frac{\partial \pi_2}{\partial t} U_t t \right)^2 \right)^{\frac{1}{2}} \quad (39)$$

Similar relationships were used to estimate the uncertainty of other calculated parameters such as porosity, surface tension, permeability, and inertial resistance. There were numerous equations, similar in form to equation 39, involved in the uncertainty analysis. In order to deal with all of the uncertainty equations, an Excel macro was written. The Excel macro and full uncertainty calculations are shown in Appendix E.

The coated and uncoated media had different porosities associated with them, based on the packed bed and fibrous matte models. Thus the calculated uncertainty for aspect ratio was also different between the coated and uncoated media. The coated and uncoated medium uncertainties were calculated assuming a packed bed and fibrous matte model respectively.

### 6.2.1 Uncertainty Results

A summary of the calculated uncertainties for all parameters associated with the aspect ratio and CFD model are listed in Table 4. These results were calculated using the procedure presented in the previous section.

Table 4: Estimated Uncertainty of Parameters

<b>Parameter</b>	<b>Uncertainty Estimates</b>
Length	+/- 0.1%
Time	+/- 0.1%
Density	+/-0.5%
Viscosity	+/-0.5%
Velocity	+/-0.16%
Surface Tension	+/-1.9%
Void Fraction/Porosity	+/-1.3%
Paper GSM	+/-0.25%
Media Sample Dry Weight	+/-0.4%
Coated Particle Diameter	+/-1%
Dimensionless Permeability	+/-2%
Uncoated Droplet Aspect Ratio ( $\pi_2$ )	+/-10.1%
Coated Droplet Aspect Ratio ( $\pi_2$ )	+/-20.5%
Uncoated Permeability (Viscous Coefficient)	+/-2.0%
Coated Permeability (Viscous Coefficient)	+/-4.8%
Uncoated Inertial Resistance	+/-3.3%
Coated Inertial Resistance	+/-3.0%

## **CHAPTER SEVEN**

### **SUMMARY AND CONCLUSIONS**

The project presented in this thesis took an in depth look into a droplet impacting with a porous medium. The resulting geometry of the droplet after impact was studied and characterized by the droplet aspect ratio. An experiment was set up to study a water droplet impacting with porous papers. Four different media were examined, with one being a porous coated medium and the remaining three composed of un-coated plain paper. A high speed camera captured the water droplet as it was ejected from a syringe nozzle and then collided with the medium. The camera images were analyzed to determine the droplet volume, velocity, and aspect ratio.

In addition to the dimensional analysis the system was modeled using the CFD software Fluent. Using the VOF and porous medium models within Fluent a model simulating the droplet system was created. The model was run to simulate the experimental data. The CFD results were then compared to the experimental results for aspect ratio. It was determined that the CFD model was unreliable immediately after impact until 0.1 seconds after impact. After this time the CFD model was able to predict the droplet aspect ratio within a range of +/- 20% compared to the experimental data. The CFD model could be further improved by trying to understand the errors associated with droplet immediately after impact. Most likely an additional term/function needs to be added to incorporate the droplet oscillation effect immediately after impact. This additional functionality would account for inertial effects caused by impact.

Both the CFD model and experimental results showed that the porous coated medium had the highest aspect ratio. This medium also had the highest porosity value, and lowest surface tension coefficient between the medium and water droplet.

A dimensional analysis was also performed for the droplet system. The resulting pi terms were used along with the experimental data to derive an equation to predict the aspect ratio. The resulting equation was able to predict the aspect ratio within a range of +/- 10% deviation from the experimental aspect ratio.

An industrial application where this type of model could be important is the design of an inkjet printer. Droplet shape, volume, placement, and absorption properties are very important in an inkjet printer. Ensuring that the printout is dry enough for a user to handle is important. Since current technology relies heavily upon absorption of the ink into the medium for drying, absorption performance is critical. A model similar to the one presented in this thesis could help to ensure that the specified droplet and medium properties have an acceptable absorption performance. A future recommendation would be to repeat the experiment and model at a droplet speed and size similar to those found in inkjet printing.

## BIBLIOGRAPHY

Alam, P., M. Toivakka, K. Backfolk, and P. Sirvio, "Impact spreading and absorption of Newtonian droplets on topographically irregular porous materials," *Chemical Engineering Science*, 62: 3142-3158 (2007).

Campbell, W.B., "The physics of water removal," *Pul Paper Mag. Can*, 48: 103-110 (1947).

Coleman, H.W. and W.G. Steele, *Experimentation and uncertainty analysis for engineers*, 1<sup>st</sup> Edition, John Wiley & Sons, New York (1989).

De Gennes, P., F. Brochard-Wyart, and D. Quere, *Capillarity and Wetting Phenomena*, Springer Publications, New York (2004).

Ergun, S., "Fluid Flow through Packed Columns," *Chemical Engineering Progress*, 48: 89-94 (1952).

FLUENT, 6.3 User's Guide, <http://www.fluentusers.com> (2007).

Hamlen, R.C. and L.E. Scriven, "Permeabilities to Fluid Flow Vary with Sheet Compression: Analysis and Model of Basics," *TAPPI Coating Conference*, Montreal, Canada (1991).

Hamraoui, A. and T. Nylander, "Analytical Approach for the Lucas-Washburn Equation," *Journal of Colloid and Interface Science*, 250: 415-421 (2002).

Hsu, N. and N. Ashgriz, "Nonlinear penetration of liquid drops into radial capillaries," *Journal of Colloid and Interface Science*, 270: 146-162 (2004).

Jackson, G.W. and D.F. James, "The Permeability of Fibrous Porous Media," *The Canadian Journal of Chem. Eng.*, 64: 364-374 (1986).

Kannangara, D., H. Zhang, and W. Shen, "Liquid-paper interactions during liquid drop impact and recoil on paper surfaces," *Colloid and Surfaces A: Physicochem. Eng. Aspects*, 280: 203-215 (2006).

Lindsay, J.D., "The anisotropic permeability of paper," *Tappi Journal*, 73: 223-229 (1990).

Marmur, A. and R.D. Cohen, "Characterization of Porous Media by the Kinetics of Liquid Penetration: The Vertical Capillaries Model," *Journal of Colloid and Interface Sciences*, 189: 299-304 (1997).

Meriam, J.L. and L.G. Kraige, *Engineering Mechanics Dynamics Fourth Edition*, John Wiley & Sons, New York (1997).

Nilsson, L. and S. Stenstrom, "A Study of the Permeability of Pulp and Paper" *Int. J. Multiphase Flow*, 23: 131-153 (1997).

Park, H., W. Carr, J. Zhu, and J. Morris, "Single Drop Impaction on a Solid Surface," *AIChE*, 49: 2461-2471 (2003).

Perry, R.H. and D.W. Green, *Perry's Chemical Engineers' Handbook Seventh Edition*, McGraw-Hill Companies, New York (1997).

Reis, N.C., R.F. Griffiths, and J.M. Santos, "Numerical simulation of the impact of liquid droplets on porous surfaces," *Journal of Computational Physics*, 198: 747-770 (2004).

Rioux, R.W., "The Rate of Fluid Absorption in Porous Media," The University of Maine (2003).

Wilcox, D.C., "*Turbulence modeling for CFD*," DCW Industries, Inc, California (1993).

Young, D.F., B.R. Munson, and T.H. Okiishi, *A Brief Introduction to Fluid Mechanics*, John Wiley & Sons, New York (1997).

## APPENDIX A

### A. Inertial Resistance for Uncoated Media

An inertial resistance coefficient,  $C_2$ , for the plate is defined as:

$$C_2 = \frac{K'_L}{L_m} \quad (1a)$$

The adjusted loss factor can be related to the velocity and loss factor for a region of equal area that is completely open to flow.

$$K'_L = K_L \left( \frac{v_{pb}}{v_{open}} \right) \quad (2a)$$

Figure 5 shows the two areas:

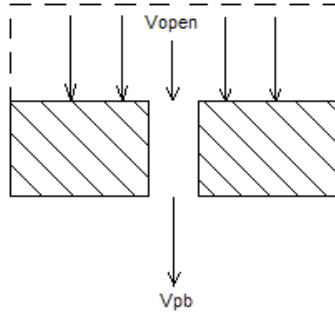


Figure 1a: Velocity of the 100% open and partially block areas.

Based on the conservation of mass principle and the continuity equation for incompressible flow, the two areas for completely open and partially blocked flow would have the same flow rate. Assuming the flow rates are equal, the velocity in the porous region can be related to the velocity in the open region by the void fraction of the medium.

$$v_{pb} = \frac{v_{open}}{\varepsilon} \quad (3a)$$

Substituting equations 12 and 13 into equation 11, the inertial resistance coefficient is defined as:

$$C_2 = \frac{K_L}{L_m} \left( \frac{1}{\varepsilon} \right)^2 \quad (4a)$$



## APPENDIX B

### B. Surface Tension at Substrate/Air Interface

In order to estimate the surface tension at the substrate/air interface, we can look at the case of two semi-infinite substrates in contact with each other. The surface energy of the two substrates when not in contact with each other, but in contact with the air between the substrates, is equal to  $2\sigma_{SA}$ . When in contact with each other, the surface energy is equal to the van der Waals energy between the two substrates.

$$2\sigma_{SA} - V_{SS} = 0 \quad (1b)$$

$$\sigma_{SA} = \frac{V_{SS}}{2} \quad (2b)$$

The van der Waals energy is defined as:

$$V_{SS} = k * a_s^2 \quad (3b)$$

The spreading parameter,  $S$ , can be related to the van der Waals interactions through the following relationship:

$$S = V_{SL} - V_{LL} \quad (4b)$$

The spreading parameter can also be related to the contact angle,  $\theta$ .

$$S = \sigma_{LA} (\cos\theta - 1) \quad (5b)$$

Substituting equation 5b into equation 4b results in the following equation:

$$\sigma_{LA} (\cos\theta - 1) = V_{SL} - V_{LL} \quad (6b)$$

For two semi-infinite identical liquids:

$$2\sigma_{LA} - V_{LL} = 0 \quad (7b)$$

$$V_{LL} = 2\sigma_{LA} \quad (8b)$$

The van der Waals energy can also be defined as:

$$V_{LL} = k * a_L^2 \quad (9b)$$

Substituting equation 9b into equation 8b results in the following relationship for electric polarisability of the liquid:

$$a_L = \sqrt{\frac{2\sigma_{LA}}{k}} \quad (10b)$$

For the substrate/liquid interface the van der Waals energy is defined as:

$$V_{SL} = k * a_S * a_L \quad (11b)$$

$$a_S = \frac{V_{SL}}{k * a_L} \quad (12b)$$

Substituting equation 12b into equation 3b resulting in the following equation:

$$V_{SS} = k \left( \frac{V_{SL}}{k * a_L} \right)^2 \quad (13b)$$

Rearranging equation 6b and inserting it into equation 13b, along with equation 10b, results in the following equation:

$$V_{SS} = k \left( \frac{[\sigma_{LA}(\cos\theta - 1) + V_{LL}]}{k \sqrt{\frac{2\sigma_{LA}}{k}}} \right)^2 \quad (14b)$$

$$V_{SS} = \left( \frac{[\sigma_{LA}(\cos\theta - 1) + V_{LL}]^2}{2\sigma_{LA}} \right) \quad (15b)$$

Substituting equation 8b into equation 15b results in the following relationship:

$$V_{SS} = \frac{[\sigma_{LA}(\cos\theta - 1) + 2\sigma_{LA}]^2}{2\sigma_{LA}} \quad (16b)$$

$$V_{SS} = \frac{\gamma_{LA}(\cos\theta + 1)^2}{2} \quad (17b)$$

Substituting equation 17b into equation 2b results in the following equation for the surface tension at the substrate/air interface:

$$\gamma_{SA} = \frac{\gamma_{LA}(\cos\theta + 1)^2}{4} \quad (18b)$$

## APPENDIX C

### C. Dimensional Analysis

Important Variables =  $f(h, d, H, D, V, \rho, \mu, \sigma, \epsilon, t)$

Basic Units = M (mass), L (length), T (time)

Repeating Variables: D, V,  $\mu$

# Variables = 10

# Repeating Variables = 3

# Pi Terms =  $10 - 3 = 7$

$$\pi_1 = hD^a V^b \mu^c$$

$$M^0 L^0 T^0 = L(L)^a \left(\frac{L}{T}\right)^b \left(\frac{M}{LT}\right)^c$$

$$a = -1$$

$$b = 0$$

$$c = 0$$

$$\pi_1 = \frac{h}{D}$$

$$\pi_2 = dD^a V^b \mu^c$$

$$M^0 L^0 T^0 = L(L)^a \left(\frac{L}{T}\right)^b \left(\frac{M}{LT}\right)^c$$

$$a = -1$$

$$b = 0$$

$$c = 0$$

$$\pi_2 = \frac{d}{D}$$

$$\pi_3 = HD^a V^b \mu^c$$

$$M^0 L^0 T^0 = L(L)^a \left(\frac{L}{T}\right)^b \left(\frac{M}{LT}\right)^c$$

$$a = -1$$

$$b = 0$$

$$c = 0$$

$$\pi_3 = \frac{H}{D}$$

$$\pi_4 = \rho D^a V^b \mu^c$$

$$M^0 L^0 T^0 = \left(\frac{M}{L^3}\right) (L)^a \left(\frac{L}{T}\right)^b \left(\frac{M}{LT}\right)^c$$

$$a = 1$$

$$b = 1$$

$$c = -1$$

$$\pi_4 = \frac{\rho V D}{\mu} = \text{Re}$$

$$\pi_5 = \sigma D^a V^b \mu^c$$

$$M^0 L^0 T^0 = \left(\frac{M}{T^2}\right) (L)^a \left(\frac{L}{T}\right)^b \left(\frac{M}{LT}\right)^c$$

$$a = 0$$

$$b = -1$$

$$c = -1$$

$$\pi_5 = \frac{\sigma}{V\mu}$$

$$\pi_6 = \varepsilon D^a V^b \mu^c$$

$$a=0$$

$$b=0$$

$$c=0$$

$$\pi_6 = \varepsilon$$

$$\pi_7 = tD^a V^b \mu^c$$

$$M^0 L^0 T^0 = T(L)^a \left(\frac{L}{T}\right)^b \left(\frac{M}{LT}\right)^c$$

$$a=-1$$

$$b=1$$

$$c=0$$

$$\pi_7 = \frac{tV}{D}$$

The aspect ratio ( $r$ ) is equal to  $\pi_2/\pi_1$ .

$$r = \frac{\pi_2}{\pi_1} = \frac{\frac{d}{D}}{\frac{h}{D}} = \frac{d}{h}$$

The aspect ratio,  $r$ , will be substituted into the dimensional analysis for  $\pi_2$ .

$$\pi_2 = r = \frac{d}{h}$$

The term  $\pi_4$  can be divided by  $\pi_5$  in order to produce the Weber number.

$$We = \frac{\pi_4}{\pi_5} = \frac{\frac{\rho VD}{\mu}}{\frac{\sigma}{V\mu}} = \frac{\rho V^2 D}{\sigma}$$

The Weber number will be substituted for  $\pi_5$ .

$$\pi_5 = We = \frac{\rho V^2 D}{\sigma}$$

The term  $\pi_7$  can be divided by  $\pi_3$  to create the following parameter,  $\tau$ .

$$\tau = \frac{\pi_7}{\pi_3} = \frac{\frac{tV}{D}}{\frac{H}{D}} = \frac{tV}{H}$$

The parameter  $\tau$  will be substituted into the analysis for  $\pi_7$ .

$$\pi_7 = \tau = \frac{tV}{H}$$

## APPENDIX D

### D. Aspect Ratio Correlation

Aspect Ratio Worksheet:

**Aspect Ratio:**

$$\pi_2 = C \pi_1^{a_1} \pi_3^{a_3} \pi_4^{a_4} \pi_5^{a_5} \pi_6^{a_6} \pi_7^{a_7}$$

**Known's:**

$$\pi_1, \pi_3, \pi_4, \pi_5, \pi_6, \pi_7$$

**Variables:**

$$C, a_1, a_3, a_4, a_5, a_6, a_7$$

**System Equations:**

$$f_i = \frac{C \pi_1^{a_1} \pi_3^{a_3} \pi_4^{a_4} \pi_5^{a_5} \pi_6^{a_6} \pi_7^{a_7}}{\pi_2} - 1 = 0$$

**Optimization Equation (Sum of the Squares):**

$$\sum_{i=1}^{32} f_i^2 = 0$$

i	fi^2	fi	Knowns						
			π1	π2	π3	π4	π5	π6	π7
1	0.0006	-0.02	0.50	2.50	1.75	1002.98	0.31	0.56	4.35
2	0.0011	-0.03	0.46	2.82	1.75	1002.98	0.31	0.56	10.86
3	0.0004	-0.02	0.46	2.73	1.75	1002.98	0.31	0.56	21.73
4	0.0015	-0.04	0.46	2.73	1.75	1002.98	0.31	0.56	43.45
5	0.0041	0.06	0.43	2.80	1.87	949.47	0.37	0.62	4.19
6	0.0000	0.00	0.43	2.90	1.87	949.47	0.37	0.62	10.48
7	0.0001	0.01	0.39	3.33	1.87	949.47	0.37	0.62	20.96
8	0.0032	0.06	0.35	3.75	1.87	949.47	0.37	0.62	41.92
9	0.0002	0.02	0.29	5.29	1.75	1012.76	1.11	0.79	4.39
10	0.0000	0.00	0.27	5.85	1.75	1012.76	1.11	0.79	10.97
11	0.0016	-0.04	0.27	6.00	1.75	1012.76	1.11	0.79	21.94
12	0.0002	-0.01	0.25	6.50	1.75	1012.76	1.11	0.79	43.88
13	0.0071	0.08	0.48	2.44	1.35	1055.98	0.23	0.31	4.34
14	0.0007	0.03	0.48	2.52	1.35	1055.98	0.23	0.31	10.84

15	0.0000	0.00	0.46	2.69	1.35	1055.98	0.23	0.31	21.68
16	0.0000	0.00	0.45	2.80	1.35	1055.98	0.23	0.31	43.35
17	0.0047	-0.07	0.55	2.17	2.50	850.84	0.22	0.31	4.18
18	0.0001	-0.01	0.50	2.27	2.50	850.84	0.22	0.31	10.45
19	0.0007	-0.03	0.50	2.27	2.50	850.84	0.22	0.31	20.90
20	0.0000	0.01	0.45	2.50	2.50	850.84	0.22	0.31	41.79
21	0.0047	-0.07	0.53	2.22	2.88	694.07	0.16	0.31	3.64
22	0.0004	0.02	0.47	2.38	2.88	694.07	0.16	0.31	9.09
23	0.0000	0.00	0.47	2.38	2.88	694.07	0.16	0.31	18.19
24	0.0003	-0.02	0.47	2.38	2.88	694.07	0.16	0.31	36.38
25	0.0001	-0.01	0.54	2.14	1.96	862.45	0.19	0.31	3.87
26	0.0006	-0.02	0.50	2.38	1.96	862.45	0.19	0.31	9.67
27	0.0000	0.00	0.46	2.58	1.96	862.45	0.19	0.31	19.33
28	0.0003	-0.02	0.46	2.58	1.96	862.45	0.19	0.31	38.66
29	0.0001	0.01	0.62	1.50	4.92	613.43	0.20	0.31	4.38
30	0.0002	-0.02	0.62	1.50	4.92	613.43	0.20	0.31	10.95
31	0.0029	0.05	0.62	1.38	4.92	613.43	0.20	0.31	21.91
32	0.0011	0.03	0.62	1.38	4.92	613.43	0.20	0.31	43.81

Variables

C	a1	a2	a3	a4	a5	a6	a7
0.33	-1.6	-1	0.09	0.13953	-0.1	0.03	-0.03

Constraints

a4	>=	0
a4	<=	1

Optimal Equation

0.037



## APPENDIX E

### E. Visual Basic Code for Uncertainty

```
Sub Pi2_Uncoated_Uncertainty()  
Dim jRow As Integer  
Dim D, p, V, s, E, hd, H, u, t As Variant  
Dim dD, Dp, dV, ds, dE, dhd, dH, du, dt As Variant  
Dim UD, Up, UV, Us, UE, Uhd, UH, Uu, Ut As Variant  
Dim Td, UTd, Gst, UGst, O, UO As Variant  
Dim Wd, UWd, Lm, ULm, Ls, ULs, pf, Upf As Variant  
Dim Pi2, Upi2 As Variant  
  
Sheets("Uncoated_Data").Select  
  
For jRow = 0 To 27  
    'Get Variables:  
    D = Range("I12").Offset(jRow, 0)  
    p = Range("H5")  
    V = Range("E12").Offset(jRow, 0)  
    s = Range("G12").Offset(jRow, 0)  
    E = Range("F12").Offset(jRow, 0)  
    hd = Range("L12").Offset(jRow, 0)  
    H = Range("J12").Offset(jRow, 0)  
    u = Range("H6")  
    t = Range("C12").Offset(jRow, 0)  
  
    'Find pi2 term derivatives:  
    dD = 0.569 * ((D ^ 0.735 * p ^ 0.0889 * V ^ 0.0106 * s ^ 0.0506 * E ^ 0.0302) /  
    (hd ^ 1.56 * H ^ 0.0584 * u ^ 0.1395 * t ^ 0.0277))  
    Dp = 0.029 * ((D ^ 1.735 * p ^ -0.9111 * V ^ 0.0106 * s ^ 0.0506 * E ^ 0.0302) /  
    (hd ^ 1.56 * H ^ 0.0584 * u ^ 0.1395 * t ^ 0.0277))  
    dV = 0.0035 * ((D ^ 1.735 * p ^ 0.0889 * V ^ -0.9894 * s ^ 0.0506 * E ^ 0.0302) /  
    (hd ^ 1.56 * H ^ 0.0584 * u ^ 0.1395 * t ^ 0.0277))  
    ds = 0.0166 * ((D ^ 1.735 * p ^ 0.0889 * V ^ 0.0106 * s ^ -0.9494 * E ^ 0.0302) /  
    (hd ^ 1.56 * H ^ 0.0584 * u ^ 0.1395 * t ^ 0.0277))  
    dE = 0.0099 * ((D ^ 1.735 * p ^ 0.0889 * V ^ 0.0106 * s ^ 0.0506 * E ^ -0.9698) /  
    (hd ^ 1.56 * H ^ 0.0584 * u ^ 0.1395 * t ^ 0.0277))  
    dhd = -0.512 * ((D ^ 1.735 * p ^ 0.0889 * V ^ 0.0106 * s ^ 0.0506 * E ^ 0.0302) /  
    (hd ^ 2.56 * H ^ 0.0584 * u ^ 0.1395 * t ^ 0.0277))  
    dH = -0.019 * ((D ^ 1.735 * p ^ 0.0889 * V ^ 0.0106 * s ^ 0.0506 * E ^ 0.0302) /  
    (hd ^ 1.56 * H ^ 1.0584 * u ^ 0.1395 * t ^ 0.0277))  
    du = -0.0458 * ((D ^ 1.735 * p ^ 0.0889 * V ^ 0.0106 * s ^ 0.0506 * E ^ 0.0302) /  
    (hd ^ 1.56 * H ^ 0.0584 * u ^ 1.1395 * t ^ 0.0277))
```

$$dt = -0.009 * ((D ^ 1.735 * p ^ 0.0889 * V ^ 0.0106 * s ^ 0.0506 * E ^ 0.0302) / (hd ^ 1.56 * H ^ 0.0584 * u ^ 0.1395 * t ^ 1.0277))$$

'Uncertainties:

$$UD = 0.001 * D$$

$$Up = 0.005 * p$$

$$Uhd = 0.001 * hd$$

$$UH = 0.001 * H$$

$$Uu = 0.005 * u$$

$$Ut = 0.001 * t$$

'Velocity Uncertainty:

$$Td = \text{Range("K12").Offset(jRow, 0)}$$

$$UTd = 0.001 * Td$$

$$UV = (1 / V) * ((UH / Td) ^ 2 + ((H * UTd) / Td ^ 2) ^ 2) ^ (1 / 2)$$

'Surface Tension Uncertainty:

$$Gst = \text{Range("H7")}$$

$$O = \text{Range("M12").Offset(jRow, 0)} * (3.14 / 180)$$

$$UGst = 0.005 * Gst$$

$$UO = 0.001 * O$$

$$Us = (1 / s) * (((UO * Gst * \text{Sin}(O) * (\text{Cos}(O) - 1)) / 2) ^ 2 + UO ^ 2 * ((\text{Cos}(O) ^ 2 - 2 * \text{Cos}(O) + 1) ^ 2) / 16) ^ (1 / 2)$$

'Void Fraction Uncertainty:

$$Wd = \text{Range("H12").Offset(jRow, 0)}$$

$$Lm = \text{Range("D12").Offset(jRow, 0)}$$

$$Ls = \text{Range("H9")}$$

$$pf = \text{Range("H8")}$$

$$UWd = 0.004 * Wd$$

$$ULm = 0.001 * Lm$$

$$ULs = 0.001 * Ls$$

$$Upf = 0.005 * pf$$

$$UE = (1 / E) * ((UWd / (Lm * Ls ^ 2 * pf)) ^ 2 + ((ULm * Wd) / (Lm ^ 2 * Ls ^ 2 * pf)) ^ 2 + 4 * ((Wd * ULs) / (Lm * Ls ^ 3 * pf)) ^ 2 + ((Wd * Upf) / (Lm * Ls ^ 2 * pf ^ 2)) ^ 2) ^ (1 / 2)$$

'Pi2 Uncertainty:

$$Pi2 = \text{Range("N12").Offset(jRow, 0)}$$

$$Upi2 = (1 / Pi2) * ((dD * UD) ^ 2 + (Dp * Up) ^ 2 + (dV * UV) ^ 2 + (ds * Us) ^ 2 + (dE * UE) ^ 2 + (dhd * Uhd) ^ 2 + (dH * UH) ^ 2 + (du * Uu) ^ 2 * (dt * Ut) ^ 2) ^ (1 / 2)$$

$$\text{Range("O12").Offset(jRow, 0)} = Upi2$$

$$\text{Range("S12").Offset(jRow, 0)} = UE$$

$$\text{Range("T12").Offset(jRow, 0)} = Us$$

$$\text{Range("U12").Offset(jRow, 0)} = UV$$

Next jRow  
End Sub

Sub Uncoated\_Model\_Uncertainty()  
Dim iRow As Integer  
Dim Td, UTd, G, UG, H, UH, V, UV, Vo, UVo As Variant  
Dim a, Ua, DPerm, UDPerm, K, UK, SVoid As Variant  
Dim KL, Lm, E, UKL, ULm, UE, C2, UC2 As Variant

'Output Void Fraction & Surface Tension Uncertainties:  
Pi2\_Uncoated\_Uncertainty

For iRow = 0 To 27

'Permeability Uncertainty:

K = Range("P12").Offset(iRow, 0)  
SVoid = 1 - Range("F12").Offset(iRow, 0)  
DPerm = 1.64 \* Exp(-14.421 \* SVoid)  
UDPerm = 0.02 \* DPerm  
a = Range("R12").Offset(iRow, 0)  
Ua = 0.001 \* a  
UK = (1 / K) \* ((a ^ 2 \* UDPerm) ^ 2 + (2 \* a \* DPerm \* Ua) ^ 2) ^ (1 / 2)  
Range("V12").Offset(iRow, 0) = UK

'Inertial Resistance Uncertainty:

KL = 0.5  
UKL = 0.005 \* KL  
Lm = Range("D12").Offset(iRow, 0)  
ULm = 0.001 \* Lm  
E = Range("F12").Offset(iRow, 0)  
UE = Range("S12").Offset(iRow, 0)  
C2 = Range("Q12").Offset(iRow, 0)  
UC2 = (1 / C2) \* (((2 \* KL \* UE) / (Lm \* E ^ 3)) ^ 2 + ((KL \* ULm) / (Lm ^ 2 \* E  
^ 2)) ^ 2 + (UKL / (Lm \* E ^ 2)) ^ 2) ^ (1 / 2)  
Range("W12").Offset(iRow, 0) = UC2

Next iRow  
End Sub

Sub Pi2\_Coated\_Uncertainty()  
Dim jRow As Integer  
Dim D, p, V, s, E, hd, H, u, t As Variant  
Dim dD, Dp, dV, ds, dE, dh, dH, du, dt As Variant  
Dim UD, Up, UV, Us, UE, Uhd, UH, Uu, Ut As Variant  
Dim Td, UTd, Gst, UGst, O, UO As Variant

Dim G, UG, Lm, ULm, ps, Ups As Variant  
Dim Pi2, Upi2 As Variant

Sheets("Coated\_Data").Select

For jRow = 0 To 3

'Get Variables:

D = Sheets("Coated\_Data").Range("I12").Offset(jRow, 0)  
p = Sheets("Coated\_Data").Range("H5")  
V = Sheets("Coated\_Data").Range("E12").Offset(jRow, 0)  
s = Sheets("Coated\_Data").Range("G12").Offset(jRow, 0)  
E = Sheets("Coated\_Data").Range("F12").Offset(jRow, 0)  
hd = Sheets("Coated\_Data").Range("L12").Offset(jRow, 0)  
H = Sheets("Coated\_Data").Range("J12").Offset(jRow, 0)  
u = Sheets("Coated\_Data").Range("H6")  
t = Sheets("Coated\_Data").Range("C12").Offset(jRow, 0)

'Find pi2 term derivatives:

dD = 0.569 \* ((D ^ 0.735 \* p ^ 0.0889 \* V ^ 0.0106 \* s ^ 0.0506 \* E ^ 0.0302) /  
(hd ^ 1.56 \* H ^ 0.0584 \* u ^ 0.1395 \* t ^ 0.0277))  
Dp = 0.029 \* ((D ^ 1.735 \* p ^ -0.9111 \* V ^ 0.0106 \* s ^ 0.0506 \* E ^ 0.0302) /  
(hd ^ 1.56 \* H ^ 0.0584 \* u ^ 0.1395 \* t ^ 0.0277))  
dV = 0.0035 \* ((D ^ 1.735 \* p ^ 0.0889 \* V ^ -0.9894 \* s ^ 0.0506 \* E ^ 0.0302) /  
(hd ^ 1.56 \* H ^ 0.0584 \* u ^ 0.1395 \* t ^ 0.0277))  
ds = 0.0166 \* ((D ^ 1.735 \* p ^ 0.0889 \* V ^ 0.0106 \* s ^ -0.9494 \* E ^ 0.0302) /  
(hd ^ 1.56 \* H ^ 0.0584 \* u ^ 0.1395 \* t ^ 0.0277))  
dE = 0.0099 \* ((D ^ 1.735 \* p ^ 0.0889 \* V ^ 0.0106 \* s ^ 0.0506 \* E ^ -0.9698) /  
(hd ^ 1.56 \* H ^ 0.0584 \* u ^ 0.1395 \* t ^ 0.0277))  
dhd = -0.512 \* ((D ^ 1.735 \* p ^ 0.0889 \* V ^ 0.0106 \* s ^ 0.0506 \* E ^ 0.0302) /  
(hd ^ 2.56 \* H ^ 0.0584 \* u ^ 0.1395 \* t ^ 0.0277))  
dH = -0.019 \* ((D ^ 1.735 \* p ^ 0.0889 \* V ^ 0.0106 \* s ^ 0.0506 \* E ^ 0.0302) /  
(hd ^ 1.56 \* H ^ 1.0584 \* u ^ 0.1395 \* t ^ 0.0277))  
du = -0.0458 \* ((D ^ 1.735 \* p ^ 0.0889 \* V ^ 0.0106 \* s ^ 0.0506 \* E ^ 0.0302) /  
(hd ^ 1.56 \* H ^ 0.0584 \* u ^ 1.1395 \* t ^ 0.0277))  
dt = -0.009 \* ((D ^ 1.735 \* p ^ 0.0889 \* V ^ 0.0106 \* s ^ 0.0506 \* E ^ 0.0302) /  
(hd ^ 1.56 \* H ^ 0.0584 \* u ^ 0.1395 \* t ^ 1.0277))

'Uncertainties:

UD = 0.001 \* D  
Up = 0.005 \* p  
Uhd = 0.001 \* hd  
UH = 0.001 \* H  
Uu = 0.005 \* u  
Ut = 0.001 \* t

'Velocity Uncertainty:

Td = Sheets("Coated\_Data").Range("K12").Offset(jRow, 0)

UTd = 0.001 \* Td

UV = (1 / V) \* ((UH / Td) ^ 2 + ((H \* UTd) / Td ^ 2) ^ 2) ^ (1 / 2)

'Surface Tension Uncertainty:

Gst = Sheets("Coated\_Data").Range("H7")

O = Sheets("Coated\_Data").Range("M12").Offset(jRow, 0) \* (3.14 / 180)

UGst = 0.005 \* Gst

UO = 0.001 \* O

Us = (1 / s) \* (((UO \* Gst \* Sin(O) \* (Cos(O) - 1)) / 2) ^ 2 + UO ^ 2 \* ((Cos(O) ^ 2 - 2 \* Cos(O) + 1) ^ 2) / 16) ^ (1 / 2)

'Void Fraction Uncertainty:

G = Sheets("Coated\_Data").Range("H12").Offset(jRow, 0)

Lm = Sheets("Coated\_Data").Range("D12").Offset(jRow, 0)

ps = Sheets("Coated\_Data").Range("H8")

UG = 0.0025 \* G

ULm = 0.001 \* Lm

Ups = 0.005 \* ps

UE = (1 / E) \* ((UG / (Lm \* ps)) ^ 2 + ((G \* ULm) / (ps \* Lm ^ 2)) ^ 2 + ((Ups \* G) / (ps ^ 2 \* Lm)) ^ 2) ^ (1 / 2)

Pi2 = Sheets("Coated\_Data").Range("N12").Offset(jRow, 0)

Upi2 = (1 / Pi2) \* ((dD \* UD) ^ 2 + (Dp \* Up) ^ 2 + (dV \* UV) ^ 2 + (ds \* Us) ^ 2 + (dE \* UE) ^ 2 + (dhd \* Uhd) ^ 2 + (dH \* UH) ^ 2 + (du \* Uu) ^ 2 \* (dt \* Ut) ^ 2) ^ (1 / 2)

Sheets("Coated\_Data").Range("O12").Offset(jRow, 0) = Upi2

Sheets("Coated\_Data").Range("S12").Offset(jRow, 0) = UE

Sheets("Coated\_Data").Range("T12").Offset(jRow, 0) = Us

Sheets("Coated\_Data").Range("U12").Offset(jRow, 0) = UV

Next jRow

End Sub

Sub Coated\_Model\_Uncertainty()

Dim iRow As Integer

Dim Td, UTd, G, UG, H, UH, V, UV, Vo, UVo As Variant

Dim Dp, UDp, E, UE, K, UK As Variant

Dim C2, UC2 As Variant

'Output Void Fraction & Surface Tension Uncertainties:

Pi2\_Coated\_Uncertainty

For iRow = 0 To 3

'Permeability & Inertial Resistance Uncertainty:

K = Sheets("Coated\_Data").Range("P12").Offset(iRow, 0)

C2 = Sheets("Coated\_Data").Range("Q12").Offset(iRow, 0)

Dp = Sheets("Coated\_Data").Range("R12").Offset(iRow, 0)

E = Sheets("Coated\_Data").Range("F12").Offset(iRow, 0)

UDp = 0.01 \* Dp

UE = Sheets("Coated\_Data").Range("S12").Offset(iRow, 0)

UK = (1 / K) \* (((UDp \* Dp \* E ^ 3) / (75 \* (1 - E) ^ 2)) ^ 2 + ((UE \* Dp ^ 2 \* E ^ 2 \* (E - 3)) / (150 \* (E - 1) ^ 3)) ^ 2) ^ (1 / 2)

UC2 = (1 / C2) \* (((3.5 \* UDp \* (E - 1)) / (Dp ^ 2 \* E ^ 3)) ^ 2 + ((7 \* UE \* (E - 1.5)) / (Dp \* E ^ 4)) ^ 2) ^ (1 / 2)

Sheets("Coated\_Data").Range("V12").Offset(iRow, 0) = UK

Sheets("Coated\_Data").Range("W12").Offset(iRow, 0) = UC2

Next iRow

End Sub